Development of Diagnostics for Fusion α-particles in Deuterium-Tritium Experiments

V.G. Kiptily

and JET EFDA contributors

CCFE is the fusion research arm of the **United Kingdom Atomic Energy Authority**

CCFE
CULHAM CENTRE FOR FUSION ENERGY

Contents

1. Introduction
   - 1.1 Why should the fusion alphas be studied?
   - 1.2 What do we want to measure?
2. Nuclear reactions
   - 2.1 Fusion and diagnostic
   - 2.2 Cross-sections
   - 2.3 Fusion source spectrum
   - 2.4 Distribution function of fusion products
3. Fusion α-particle source diagnostics
   - 3.1 Neutron and γ-ray emission profiles
   - 3.2 Neutron spectrometry
4. Confined α-particle diagnostics
   - 4.1 Neutral Particle Analysers
   - 4.2 Gamma-ray diagnostics
5. Escaped α-particle diagnostics
   - 5.1 Scintillator Probe
   - 5.2 α-particle collectors
6. Summary

Introduction

1.1. Why should the fusion alphas be studied?

- Reactor plasma is self-heated by fusion α-particles
- Up to now , fusion research was in sub-critical zone, without burn or with small burn (Q^{max}=0.61, JET in 1997)

  "Fusion gain" factor Q gives the ratio of *fusion power* to the external power (NBI, ICRH, …) needed to sustain the energetic equilibrium

- Fast ions/alphas may drive MagnetoHydroDynamic instabilities and can in turn be re-distributed and, in some cases, lost
- Loss of bulk plasma heating is unacceptable for an efficient power plant
  - May lead to ignition problems
  - Damage to first wall
  - Can only tolerate fast ion losses of a few % in a reactor

Introduction

1.1. Why should the fusion alphas be studied?

Burning plasma - fundamentally new physics.

New phenomena have to be studied:

10>Q>5 : α-particle effects on MHD stability and turbulence

Q>10 : strong non-linear coupling between α's and pressure driven current, turbulent transport, MHD stability;

$Q \rightarrow \infty$: ignition transient phenomena

Introduction

1.2. What do we want to measure?

Fusion reaction rate:

Neutron and γ-ray diagnostics

Spatial α-particle distribution / redistribution effects:

Neutron and γ-ray diagnostics

α-particle energy distributions:

γ-ray and neutron spectrometry, neutral particle analyser

α-particle slowing down & confinement effects:

γ-ray diagnostics

α-particle losses:

Scintillator Probe, Faraday Cups, activation

Introduction

1.2. What do we want to measure?

ITER requirements

- Fusion α-particle source : $10^{12} - 4\times10^{18}$ n m^{-3} s^{-1} for $r/a < 0.75$

  Spatial : a/30 Time: 0.1 – 1 ms Accuracy: 10%

- Confined α-particles: $0.1 - 2\times10^{18}$ m^{-3}

  Spatial : a/10 Time: 100 ms Accuracy: 20%

- Lost α-particles: 2 - 20 MWm^{-2}

  Spatial : a/10 Time: 0.1 – 0.5 ms Accuracy: 10%

Introduction

JET is the tokamak closest to the ITER parameters with unique capabilities of tritium operation

	JET	ITER
R, m	3.1	6.2
a, m	1.0	2.0
I_P, MA	up to 5	up to 15
B_T, T	up to 4	up to 5.3

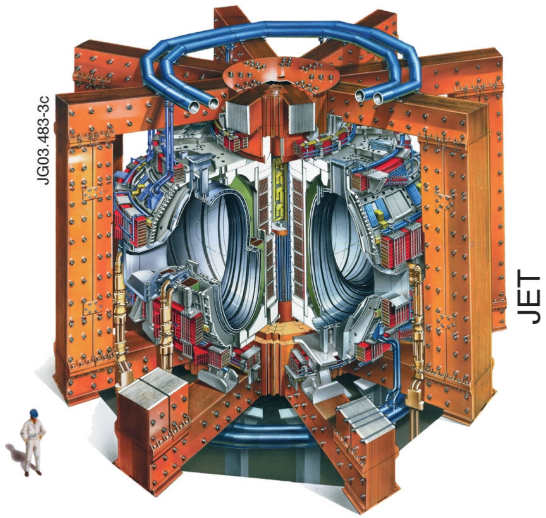

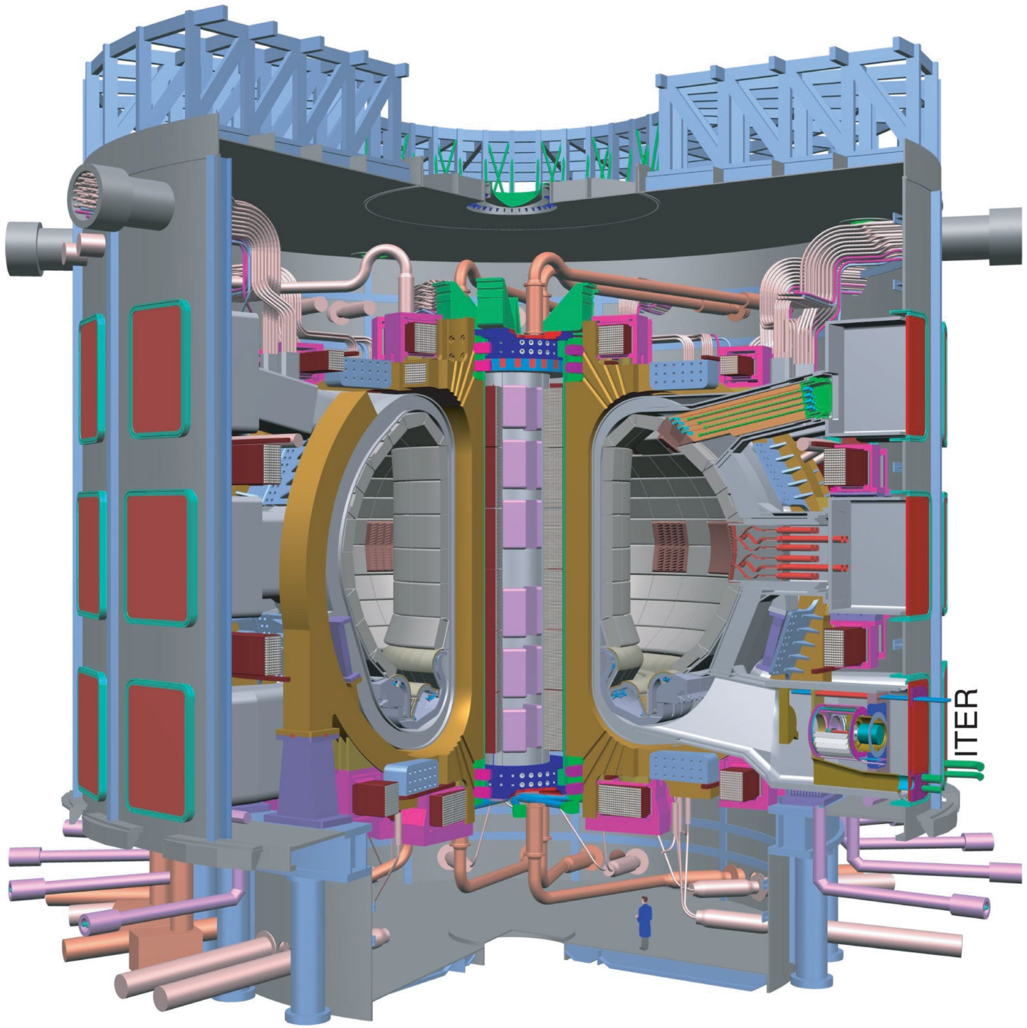

$V_{ITER} / V_{JET} \sim 10$

Introduction

In JET vessel

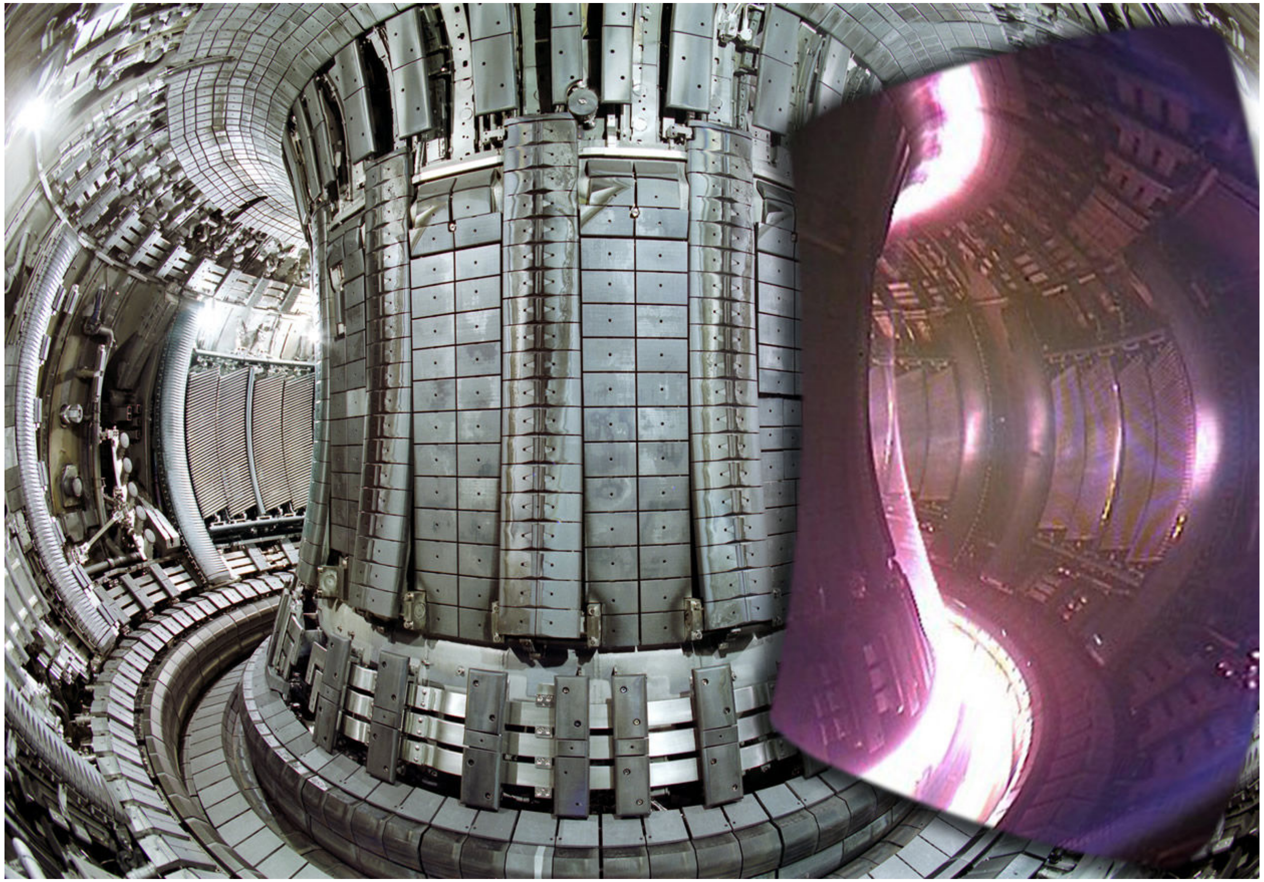

ITER-like wall: CFC tiles are replaced by Be

JET plasma heating

ICRH>8 MW

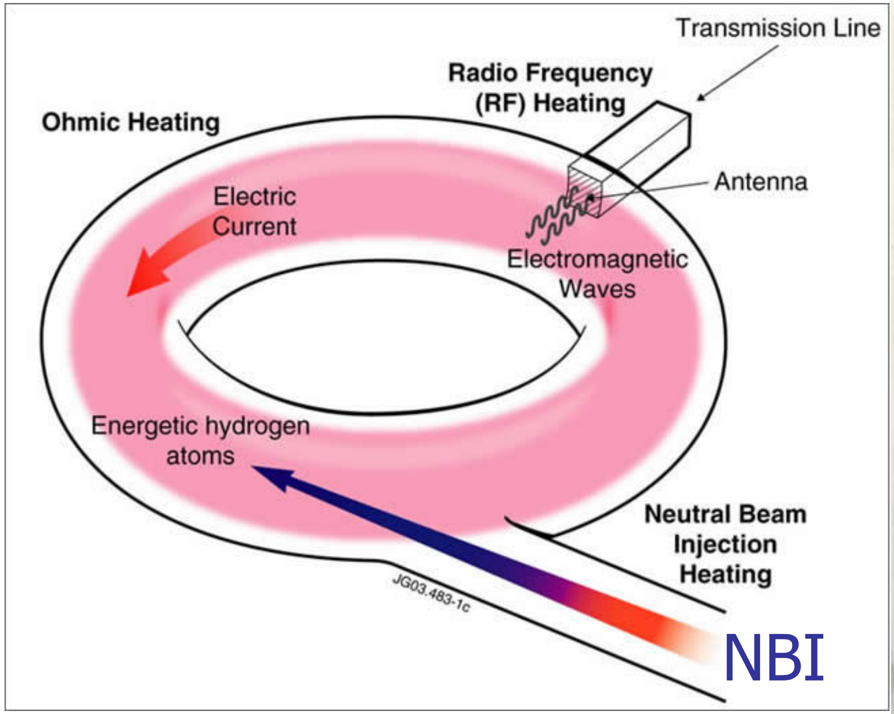

NBI

23 MW

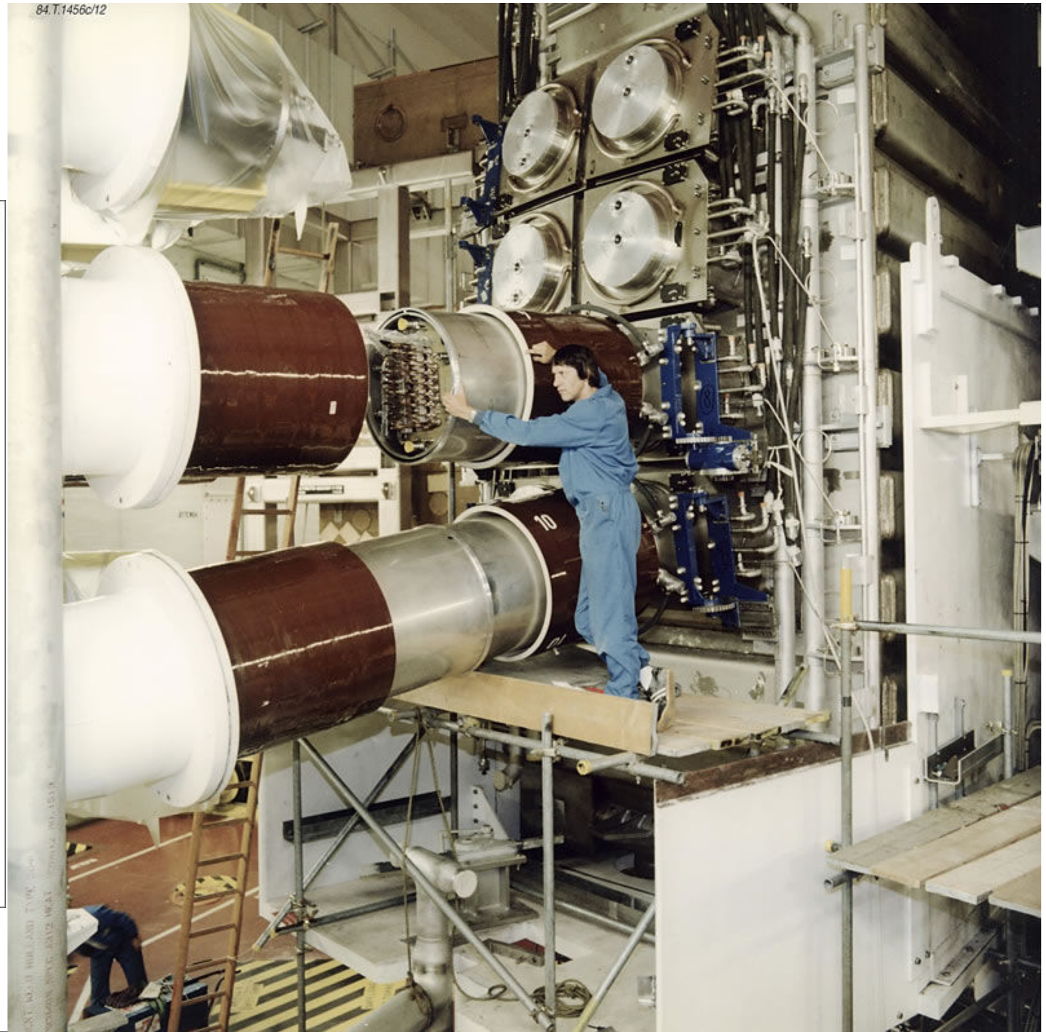

Fusion power progress (in D-T plasma)

- 1991 – JET – 1.7MW (10% T; 10MW heating)
- 1995 – TFTR – 10MW (50% T; 40MW heating)
- 1997 – JET – 16MW (50% T; 22MW heating)
- 2015? JET up to 20MW (50% T; 35MW? heating)

Main goals:

- Fuel retention, material erosion, migration and dust (containing T).
- Assessment of the influence of isotope mass
  - on access to H-mode and high confinement.
  - on edge pedestal characteristics, ELMs and their mitigation.
  - on “hybrid” and “steady state (ITB)” scenarios.
- Study of alpha particle behaviour.

Nuclear reactions

2.1. Fusion reactions: stellar

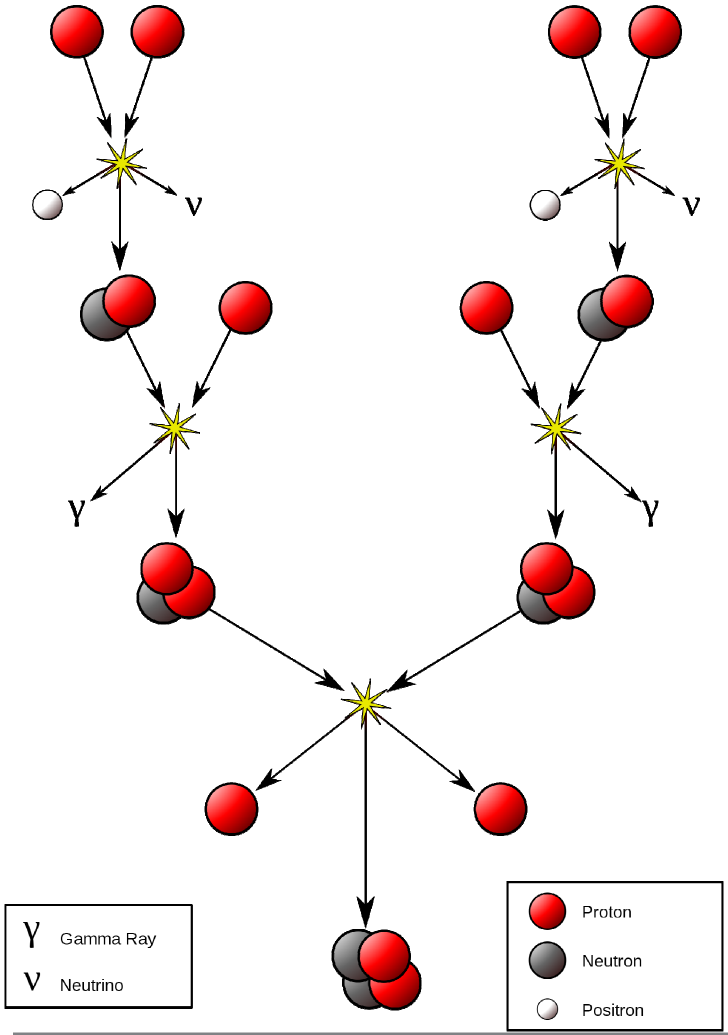

The prime energy producer in the Sun is the fusion of H to He, which occurs at a $T > 3\ 10^6$ K.

The 1st step

$H + H \rightarrow D + e^+ + \nu_e + 0.42$ MeV

The positron immediately annihilates

$e^- + e^+ \rightarrow 2\gamma + 1.02$ MeV

Then deuterium to produce ^3He:

$D + H \rightarrow {}^3He + \gamma + 5.49$ MeV

And the path to generate ^4He

${}^3He + {}^3He \rightarrow {}^4He + 2H + 12.86$ MeV

There are some other pp-chains.

This pp-chain is mostly probable in the Sun (p=0.86) and releases a net energy of 26.7 MeV.

2.1. Fusion reactions in Lab

In lab-made fusion we use reactions with larger cross-sections:

$D + D \rightarrow T\ (1.01\ \text{MeV}) + p\ (3.02\ \text{MeV})$

$\rightarrow {}^{3}He\ (0.82\ \text{MeV}) + n\ (2.45\ \text{MeV})$

$D + {}^{3}He \rightarrow {}^{4}He\ (3.6\ \text{MeV}) + p\ (14.7\ \text{MeV})$

$D + T \rightarrow {}^{4}He\ (3.5\ \text{MeV}) + n\ (14.1\ \text{MeV})$

$T + T \rightarrow {}^{4}He + 2n + 11.3\ \text{MeV}$

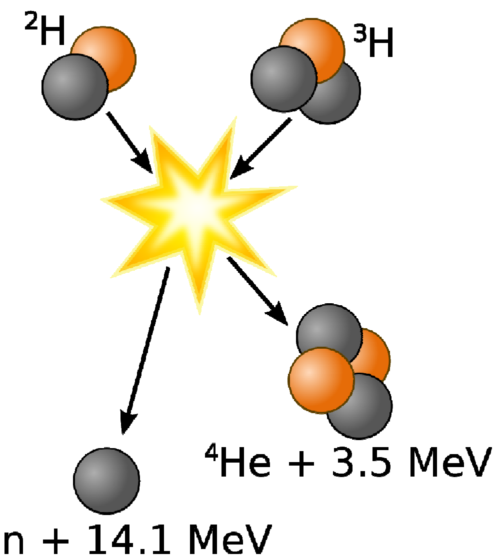

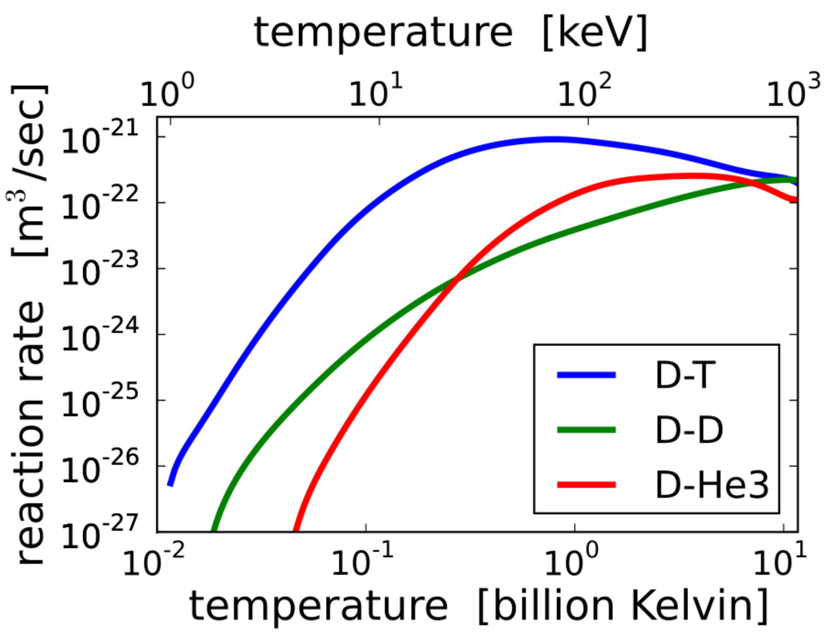

2.1. Fusion reactions: tritium production

Naturally occurring T is extremely rare, trace amounts are formed with cosmic rays in atmosphere (neutron energy > 4 MeV is needed):

$^{14}N + n \rightarrow {}^{12}C + T$

T does not accumulate - relatively short half-life ($T_{1/2} \approx 12.32$ y)

$T \rightarrow {}^{3}He + e^{-} + \nu_e + 18.6$ keV

Tritium is produced in nuclear reactors

$6Li + n \rightarrow {}^{4}He\ (2.05\ MeV) + T\ (2.75\ MeV)$

High-energy neutrons can also produce T (not attractive method)

$^{7}Li + n \rightarrow {}^{4}He + T + n + 2.466\ MeV$

$^{10}B + n \rightarrow 2\ {}^{4}He + T$

Note:

1 GW fusion reactor – 125 kg of tritium per year.

U.S. DoE: only 225 kg of tritium has been produced in USA in the period 1955 - 1996.

CCFE Culham Centre for Fusion Energy

Nuclear reactions

2.1. Diagnostic reactions

The goal is to study

- Fusion reaction products: *n, p, t,* ^{3}He and α
- ICRF-driven ions: *H, D, T,* ^{3}He and ^{4}He (in JET)

Neutron diagnostics: 2.5-MeV neutrons from DD-reaction and 14-MeV from DT

Gamma diagnostics: fast ions

γ -ray emission is produced due to nuclear reactions with fuel and with the main JET (and ITER) impurities, Be and C

protons	deuterons	tritons	^{3}He
$D(p,\gamma)^{3}He$	$^{9}Be(d,p\gamma)^{10}Be$	$T(d,\gamma)^{5}He$	$D(^{3}He,\gamma)^{5}Li$
$T(p,\gamma)^{4}He$	$^{9}Be(d,n\gamma)^{10}B$	$^{9}Be(t,n\gamma)^{11}B$	$^{9}Be(^{3}He,p\gamma)^{11}B$
$^{9}Be(p,\gamma)^{10}B$	$^{12}C(d,p\gamma)^{13}C$	$^{12}C(t,\gamma)^{15}N$	$^{9}Be(^{3}He,n\gamma)^{11}C$
$^{9}Be(p,p'\gamma)^{9}Be$		$^{12}C(t,n\gamma)^{14}N$	$^{9}Be(^{3}He,d\gamma)^{10}B$
$^{9}Be(p,\alpha\ \gamma)^{6}Li$		$^{12}C(t,\alpha\gamma)^{11}B$	$^{12}C(^{3}He,p\gamma)^{14}N$
$^{12}C(p,p'\gamma)^{12}C$			

α-particle diagnosis in JET is based on the $^{9}Be(\alpha,n\gamma)^{12}C$ reaction

2.2. Cross-sections: theoretical background

The strong energy dependence of fusion cross-sections – repulsive Coulomb potential:

Reactions are possible only because of tunnelling effect:

$$\sigma \propto \exp(-\frac{2\pi Z_1 Z_2 e^2}{\hbar V_{rel}})$$

– tunnelling probability; V_{rel} – relative velocity of the particles

Quantum mechanics shows that fusion reaction probability is also proportional to a geometrical factor:

$$\pi\lambda^2 \propto \frac{1}{E}$$

where λ – the de Broglie wavelength

Strong energy dependence → introduction of the astrophysical S-function:

$$\sigma = \mathrm{S(E)}\frac{1}{E}\exp(-\frac{B_G}{\sqrt{E}})$$

where $B_G = \pi\alpha Z_1 Z_2 \sqrt{2\mu c^2}$ is the Gamov constant; $\mu = \frac{M_1 M_2}{M_1 + M_2}$ - reduced mass;

$\alpha = e^2/\hbar c \approx 1/137$ - fine structure constant; E in keV (CM frame)

2.2. Cross-sections: parameterisation

S-function represents slowly varying nuclear part of the fusion reaction probability

S-function is important for fitting cross-section to experimental data:

$$\sigma = \frac{S(E)}{E\exp(B_G/\sqrt{E})}$$

S-function is calculated with R-matrix cross-section analysis and fitted with a Padé polynomial:

$$S(E) = \frac{A1 + E(A2 + E(A3 + E(A4 + EA5)))}{1 + E(B1 + E(B2 + E(B3 + EB4)))}$$

R-matrix theory is a mathematical description and a parameterisation of nuclear reactions: a many-body nuclear system with a short range strong forces is treated as a system with only 2-body degrees of freedom outside the ‘channel radii’.

Wigner, Eisenbud *Phys.Rev.***72***(1947)29* and Lane, Thomas *Rev.Mod.Phys.***30***(1958)257*

2.2. Cross-sections: parameterisation (2)

List of parameters for fusion cross-sections

Coefficient	$T(d,n)^4He$	$^3He(d,p)^4He$	$D(d,p)T$	$D(d,n)^3He$
B_G ($\sqrt{keV}$)	34.3827	68.7508	31.3970	31.3970
A1	6.927×10^{4}	5.7501×10^{6}	5.5576×10^{4}	5.3701×10^{4}
A2	7.454×10^{8}	2.5226×10^{3}	2.1054×10^{2}	3.3027×10^{2}
A3	2.050×10^{6}	4.5566×10^{1}	-3.2638×10^{-2}	-1.2706×10^{-1}
A4	5.2002×10^{4}	0.0	1.4987×10^{-6}	2.9327×10^{-5}
A5	0.0	0.0	1.8181×10^{-10}	-2.5151×10^{-9}
B1	6.38×10^{1}	-3.1995×10^{-3}	0.0	0.0
B2	-9.95×10^{-1}	-8.5530×10^{-6}	0.0	0.0
B3	6.981×10^{-5}	5.9014×10^{-8}	0.0	0.0
B4	1.728×10^{-4}	0.0	0.0	0.0
Energy range (keV)	0.5–550	0.3–900	0.5–5000	0.5–4900
$(\Delta S)_{max}$ (%)	1.9	2.2	2.0	2.5

E in keV; cross sections in mb ≡ 10^{-27} cm^2

Bosch, Hale *Nuclear Fusion 32(1992)611*

2.2. Cross-sections

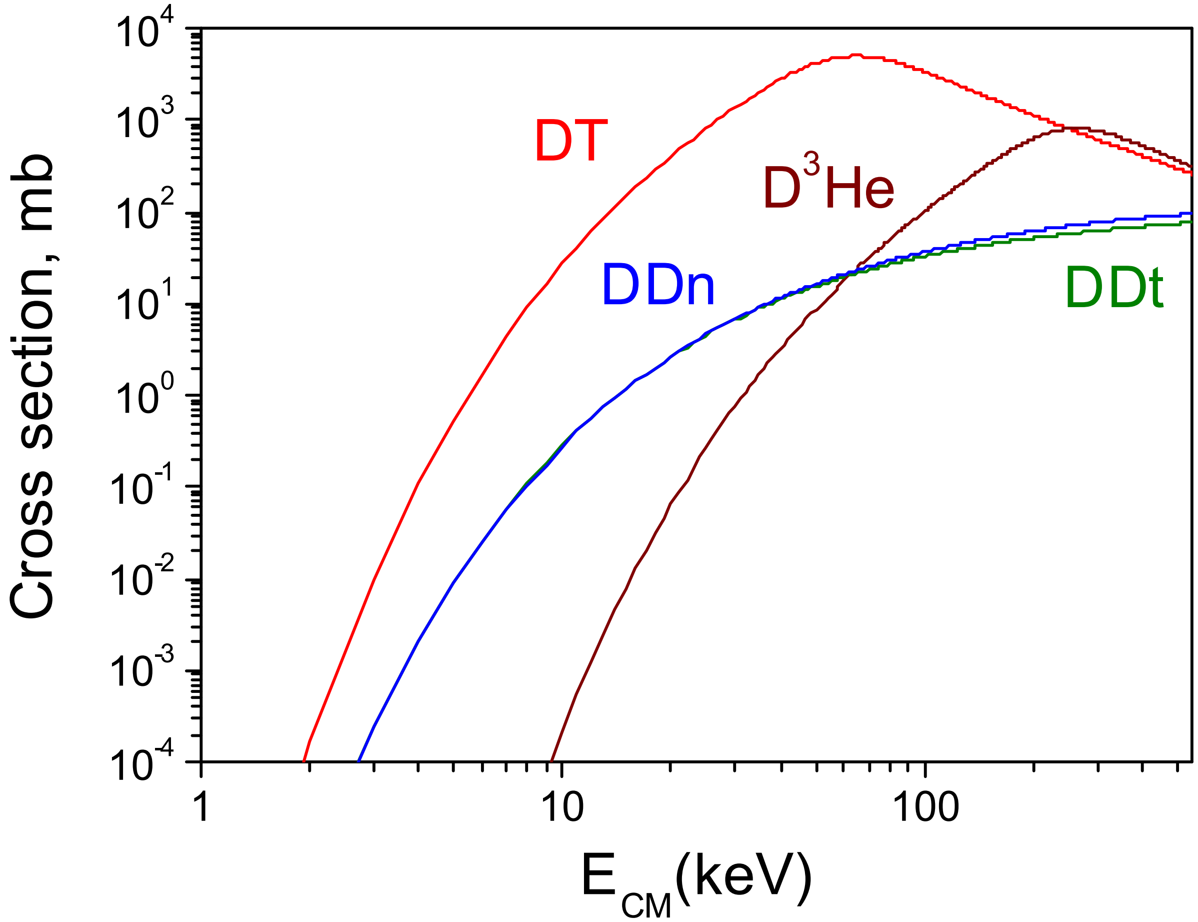

2.2. Cross-sections: fusion reactivity parameterisation

In plasma, ions have a velocity distribution, $f(\vec{V})$

and fusion rate is proportional to fusion reactivity : $R = \frac{n_i n_j}{1+\delta_{ij}} \langle \sigma v \rangle$

n_i, n_j – ion densities; fusion reactivity - $\langle \sigma v \rangle = \iint f(\vec{V}_1) f(\vec{V}_2) \sigma(|\vec{V}_1 - \vec{V}_2|) |\vec{V}_1 - \vec{V}_2| d\vec{V}_1 d\vec{V}_2$

Useful parameterisation for the fusion reactivites:

$$\langle \sigma v \rangle = C1\theta \sqrt{\xi / (\mu c^2 T^3)} e^{-3\xi}$$

$$\theta = T / \left[1 - \frac{T(C2 + T(C4 + TC6))}{1 + T(C3 + T(C5 + TC7))} \right]$$

$$\xi = (B_G^2 / (4\theta))^{1/3}$$

Peres *Nucl.Mater.50(1979)5569*

2.2. Cross-sections: fusion reactivity parameterisation (2)

List of parameters for fusion reactivities in Maxwellian plasmas

Coefficient	$T(d,n)^4He$	$^3He(d,p)^4He$	$D(d,p)T$	$D(d,n)^3He$
B_G ($\sqrt{keV}$)	34.3827	68.7508	31.3970	31.3970
m_rc^2 (keV)	1 124 656	1 124 572	937 814	937 814
C1	1.17302×10^{-9}	5.51036×10^{-10}	5.65718×10^{-12}	5.43360×10^{-12}
C2	1.51361×10^{-2}	6.41918×10^{-3}	3.41267×10^{-3}	5.85778×10^{-3}
C3	7.51886×10^{-2}	-2.02896×10^{-3}	1.99167×10^{-3}	7.68222×10^{-3}
C4	4.60643×10^{-3}	-1.91080×10^{-5}	0.0	0.0
C5	1.35000×10^{-2}	1.35776×10^{-4}	1.05060×10^{-5}	-2.96400×10^{-6}
C6	-1.06750×10^{-4}	0.0	0.0	0.0
C7	1.36600×10^{-5}	0.0	0.0	0.0
T_i range (keV)	0.2–100	0.5–190	0.2–100	0.2–100
$(\Delta\langle\sigma v\rangle)_{max}$ (%)	0.25	2.5	0.35	0.3

T is in keV; reactivity is in cm^2s^{-1}

Bosch, Hale *Nuclear Fusion 32(1992)611*

2.2. Cross-sections: fusion reactivity

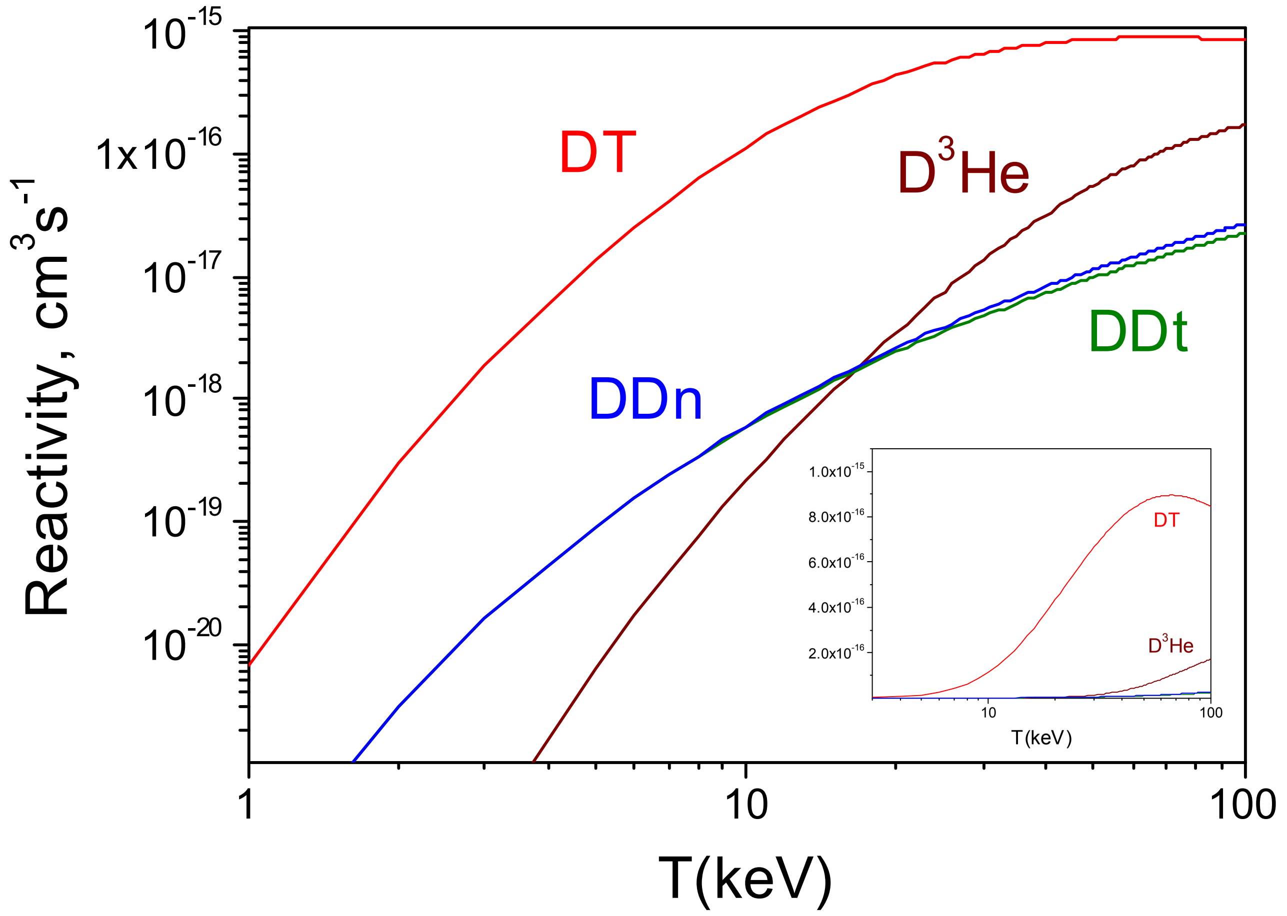

$@T = 67keV$

$\langle \sigma v \rangle_{DT} = \max$

$@T = 17keV$

$\langle \sigma v \rangle_{D^3He} = \langle \sigma v \rangle_{DDn}$

$@T = 90keV$

$\frac{\langle \sigma v \rangle_{D^3He}}{\langle \sigma v \rangle_{DDn}} \approx 6.5$

2.3. Fusion source spectrum

In the Lab system the velocity of nuclear reaction products is $\vec{v}_i = \vec{u}_i + \vec{V}_{CM}$

where $\vec{V}_{CM} = \dfrac{\vec{V}_1 M_1 + \vec{V}_2 M_2}{M_1 + M_2}$ is the velocity of CM.

The kinetic energy of the products is

$$E_i = \frac{1}{2} m_i V_{CM}{}^2 + \frac{m_j}{m_i + m_j}(Q+K) + V_{CM}\cos\theta \left[\frac{2 m_i m_j}{m_i + m_j}(Q+K)\right]^{\frac{1}{2}}$$

where $Q = M_1 + M_2 - m_i - m_j$ is the nuclear energy release of the reaction;

$K = \dfrac{1}{2}\mu V_{rel}^2$ is the relative kinetic energy with $\vec{V}_{rel} = \vec{V}_1 - \vec{V}_2$ and

$\cos\theta$ is the cosine of the angle between $\vec{V}_{rel}$ and $\vec{V}_{CM}$.

Source spectrum: $S(E_i) \propto \iiint f_1(\vec{V}_1) f_2(\vec{V}_2) \sigma(|\vec{V}_1 - \vec{V}_2|) |\vec{V}_1 - \vec{V}_2| \delta(E - E_i) d\vec{V}_1 d\vec{V}_2 d\Omega$

2.4. Distribution function of fusion products

Neutrons have an ultra weak interaction with plasmas (but interact with tokamak construction materials).

Hence, spectrum of the neutron source for Maxwellian plasmas with temperature T could be expressed as

$$\frac{dN}{dE} \propto \exp\left(-\frac{M\left(E - \langle E_{n0} \rangle\right)^2}{4 m_n T \langle E_{n0} \rangle} \right)$$

where $M = M_1 + M_2$

$$\langle E_{n0} \rangle = \frac{1}{2} m_n \langle V_{CM}{}^2 \rangle + \frac{M - m_n}{M} \left(Q + \langle K \rangle \right)$$

Therefore, temperature of the plasma could be obtained from the width (FWHM) of the spectra

$$\sigma_{DDn} = 82.3\sqrt{T} \quad \text{keV}$$

$$\sigma_{DTn} = 176.7\sqrt{T} \quad \text{keV}$$

2.4. Distribution function of fusion products (2)

Charged fusion products strongly interact with plasmas building up a distribution function. The evolution of the distribution function is defined by the Fokker-Planck equation

$$\frac{\partial f}{dt} = C + S$$

Where C represent effects of Coulomb scattering and S represents source and losses of fast particles.

If we assume that α-particles are confined $f(E) = S(E_{\alpha 0})\sqrt{\frac{E_{\alpha 0}}{E}}\frac{\sqrt{E_{\alpha 0}{}^3} + \sqrt{E_{cr}{}^3}}{\sqrt{E^3} + \sqrt{E_{cr}{}^3}}$

where $E_{cr} = 14.8 A_\alpha T_e \left\langle \frac{\sum_i n_i (Z_i^2 / A_i) \ln \Lambda_i}{n_e \ln \Lambda_e} \right\rangle^{\frac{2}{3}}$ is critical energy (for $E > E_{cr}$,

the electron drag is dominates over the bulk ion drag); Λ_e is the Coulomb logarithm.

The slowing-down time on electrons: $\tau_{se} = 2 \times 10^{10} \frac{A_\alpha T_e^{3/2}}{Z_\alpha^2 n_e \ln \Lambda_e}$

The fast ion thermalization time: $\tau_{th} = \frac{\tau_{se}}{3} \ln\left[1 + \left(\frac{E}{E_{cr}}\right)^{3/2}\right]$

2.4. Distribution function of fusion products (3)

The energy that going from ions with energy E into plasma ions is given by Stix formula

$$G_i\left(E/E_{cr}\right)=\frac{E_{cr}}{E}\int_0^{E/E_{cr}}\frac{d(E/E_{cr})}{1+(E/E_{cr})^{3/2}}$$

For fusion alpha-particles in DT plasmas

at T_e=10 keV $E_{cr}\approx$ 370 keV

~20% of alpha energy transfer to bulk ions

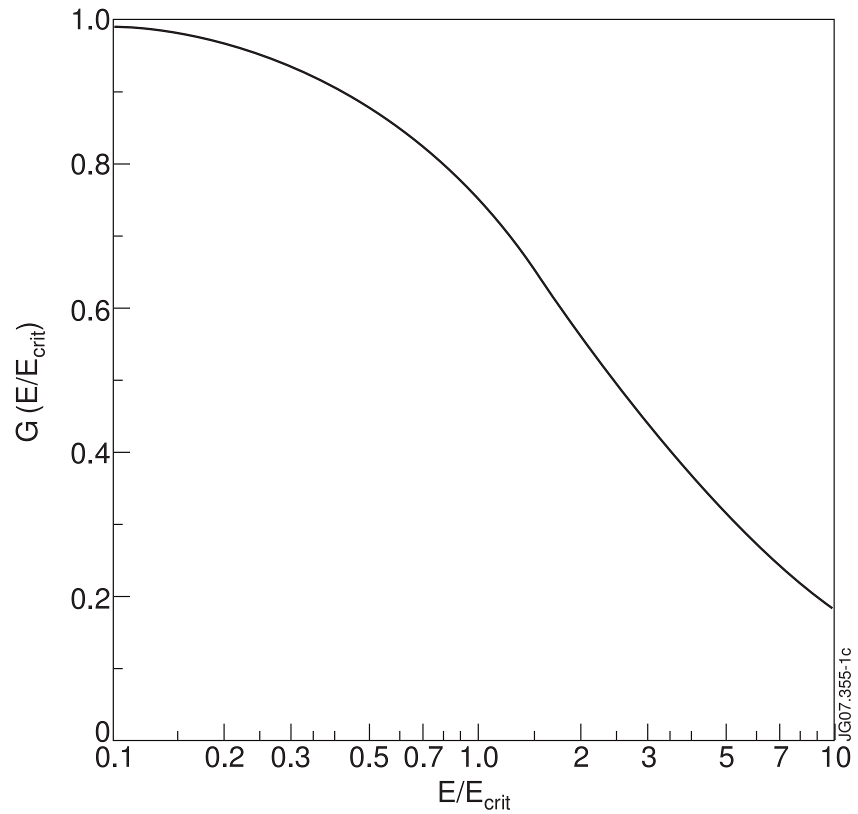

JET diagnostics

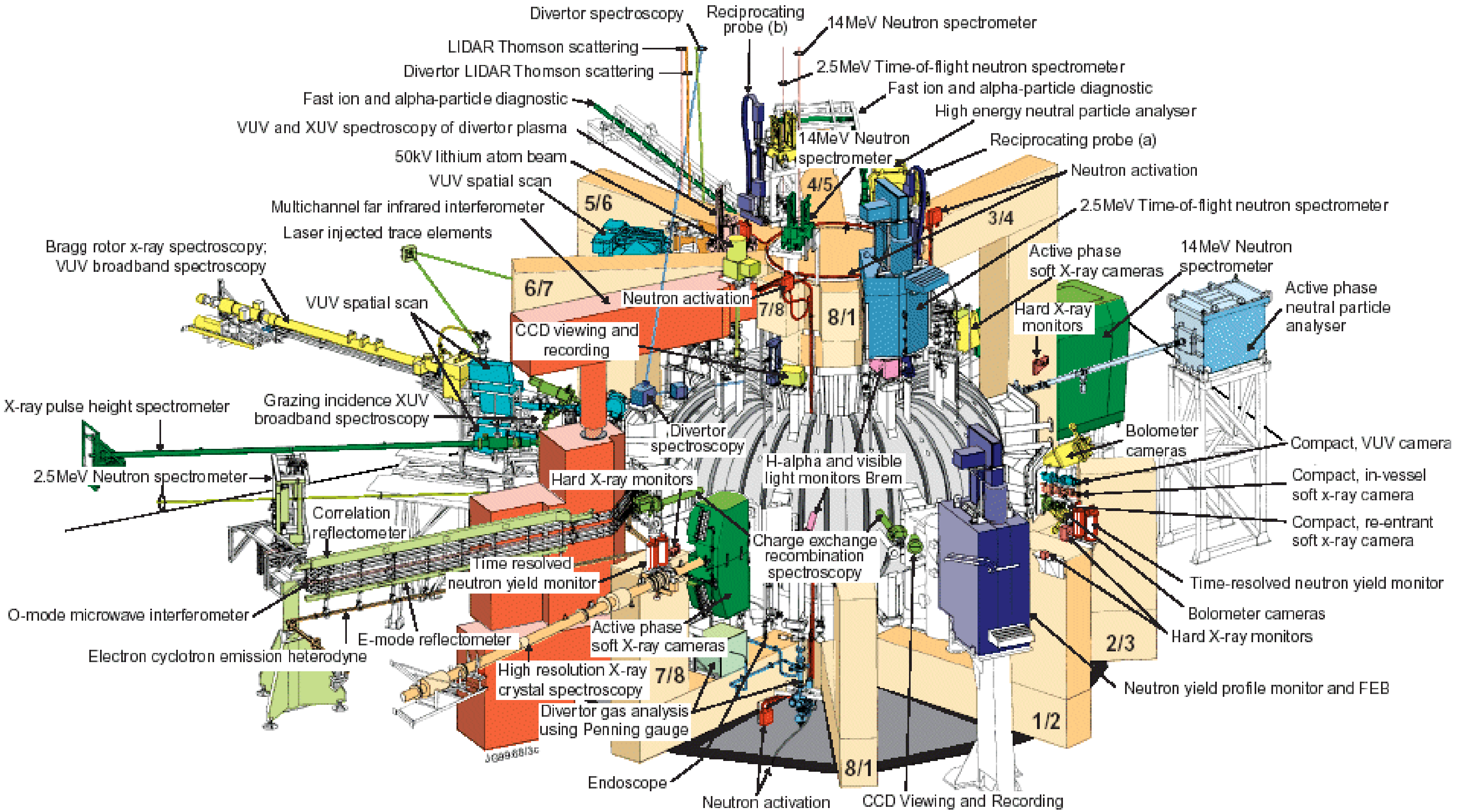

About 90 diagnostics at JET

Fusion alpha source diagnostics

3.1. Neutron emission profile

Two cameras

Vertical: 9 lines-of-sight
Horizontal: 10 lines-of-sight

Fan-shaped array of remotely adjustable collimators with two apertures (Ø10 & 21 mm)
Space resolution: ~8 (or ~15)cm (in the centre)

Detectors:
- NE213 liquid scintillators (2.5 & 14 MeV)
- Bicron-418 plastic scintillators (14 MeV)
-CsI(TI) photo-diodes (hard X-rays and γ-rays)
Neutron detectors are absolutely calibrated

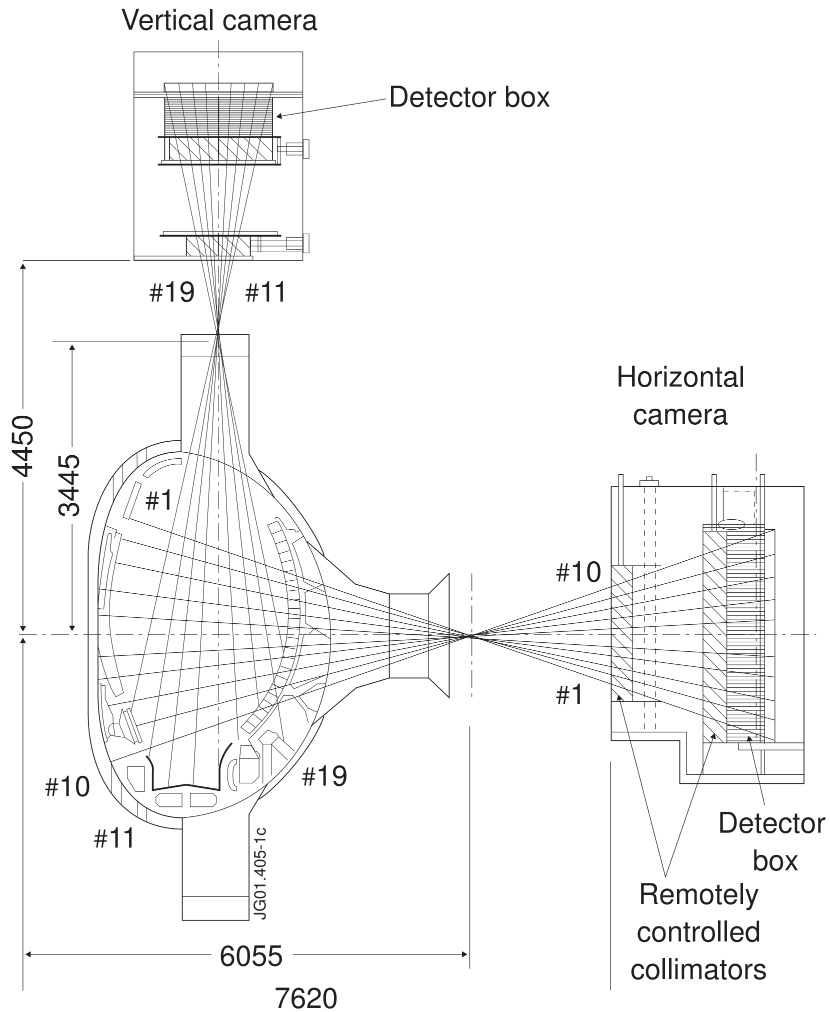

Fusion alpha source diagnostics

3.1. Neutron emission profile

Tomographic reconstruction of 14-MeV neutron measurements

Orbit calculations

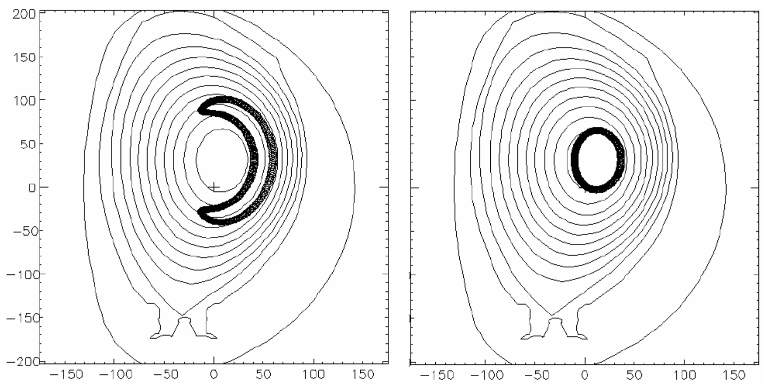

off-axis T-beam   on-axis T-beam

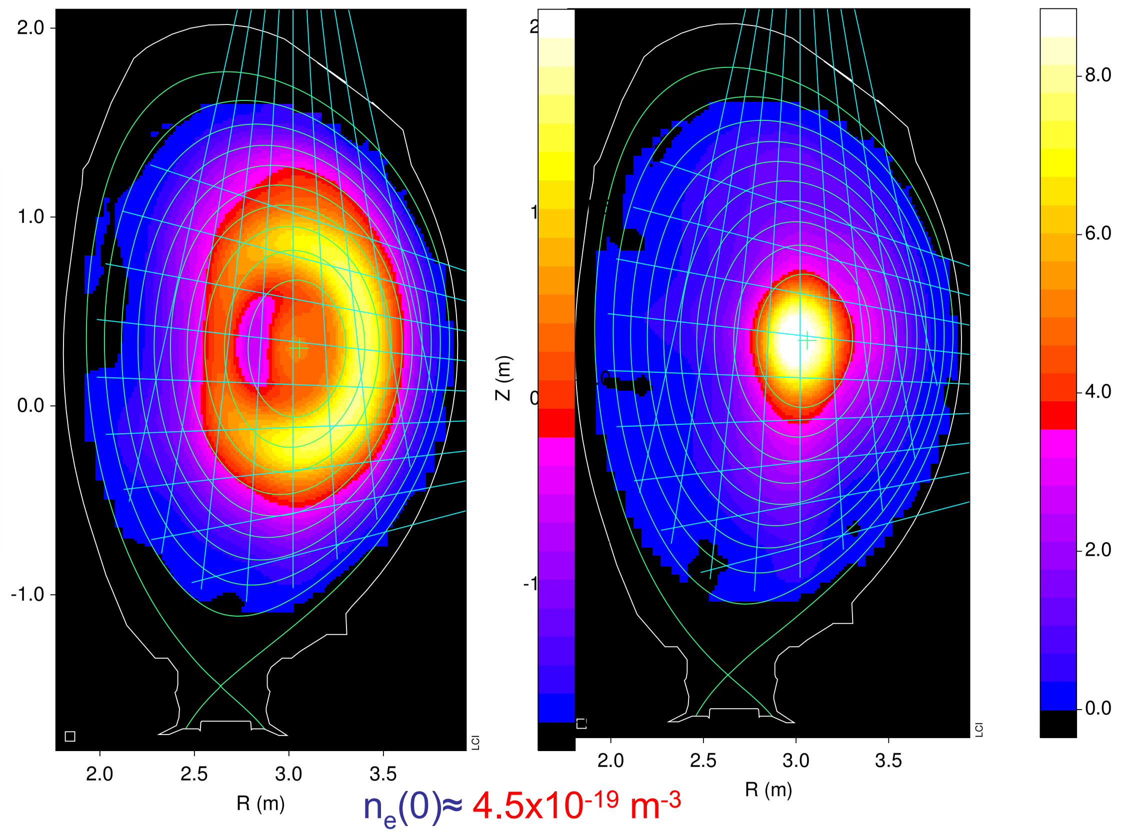

$n_e(0) \approx 4.5 \times 10^{-19}\ m^{-3}$

Fusion alpha source diagnostics

3.1. Neutron emission profile

Simulated and measured 14-MeV neutrons

TRANSP

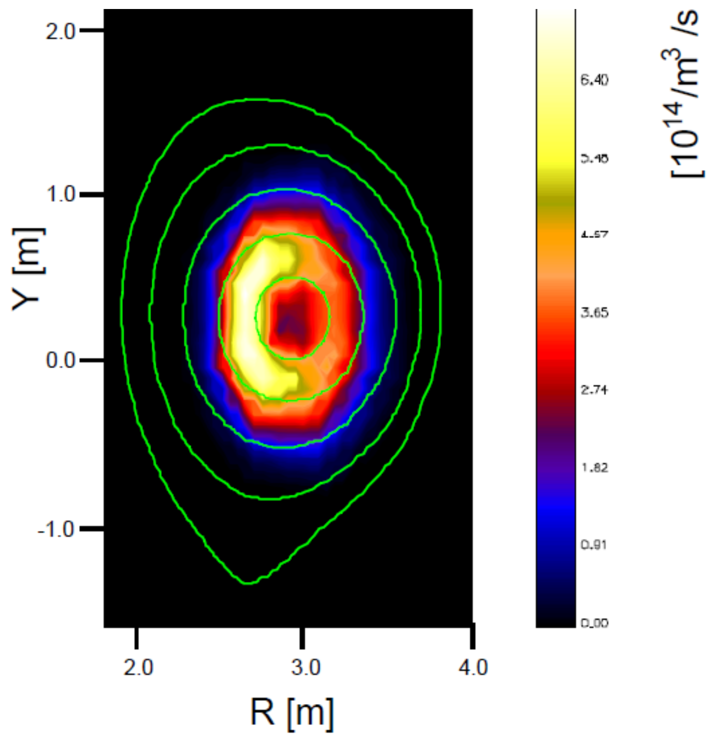

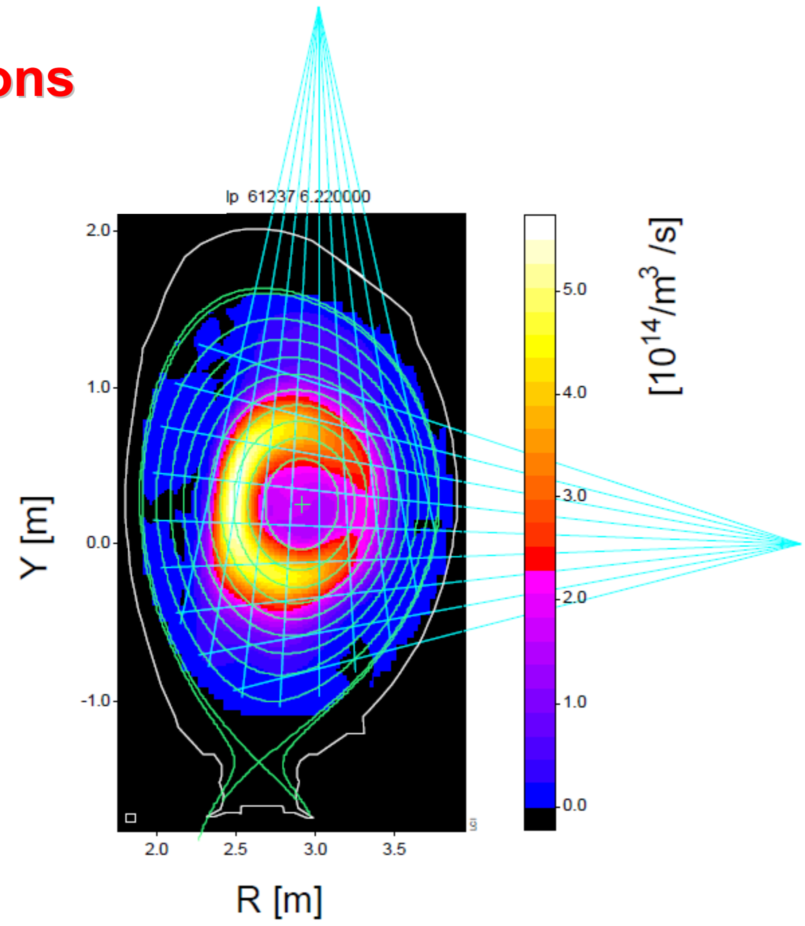

$D_{fast} = 0.4\ m^2\ /s$ R. Budny

off-axis T-beam, $n_e(0) \approx 1.8 \times 10^{-19}\ m^{-3}$

Fusion alpha source diagnostics

3.1. Fusion γ -ray emission profile

Fusion α-particle source can be measured with radiation capture reaction – branch of the main fusion reactions D+T = α + n and D+^{3}He = α + p :

D + T → ^{5}He + γ (Q=16.63 MeV) and

D + ^{3}He → ^{5}Li + γ (Q=16.38 MeV)

The branching ratio is small: $$\frac{\sigma(\gamma)}{\sigma(\alpha+n)} \approx \frac{\sigma(\gamma)}{\sigma(\alpha+p)} \approx 5\times10^{-5}$$

Nevertheless, the γ-ray profile measurements are feasible for the ITER-like reactors.

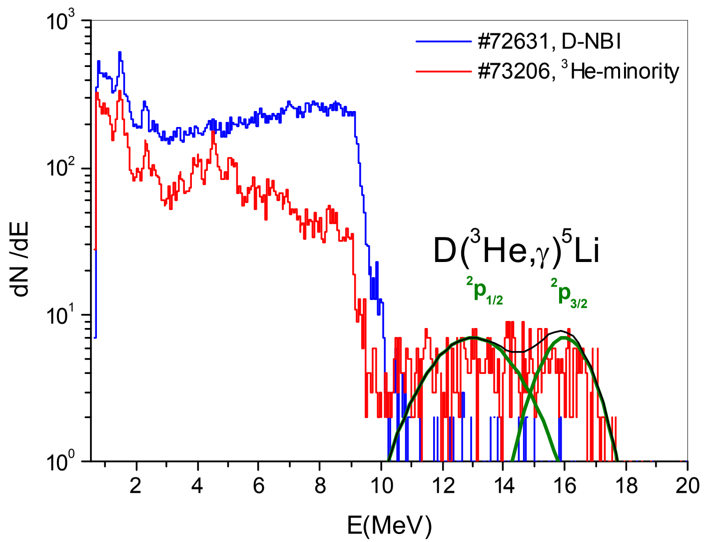

The gamma-ray spectrum recorded in the JET discharge with ^{3}He-minority heating of the D-plasma.

2 broad peaks are related to the different final states in ^{5}Li nucleus.

Also, p + T → ^{4}He + γ (Q=19.81 MeV), branch~0.05!

Fusion alpha source diagnostics

3.2. Neutron spectrometry

Magnetic Proton Recoil Ugraded spectrometer for DD- or DT-neutrons

Goal: measurements of plasma temperature (steady state) and energy distribution of the fuel ions (heating); n_D/n_T ratio.

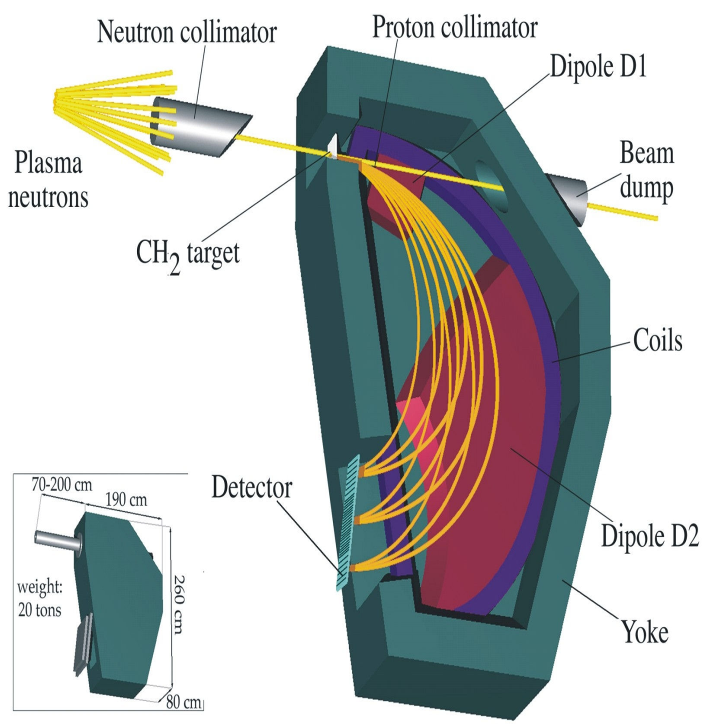

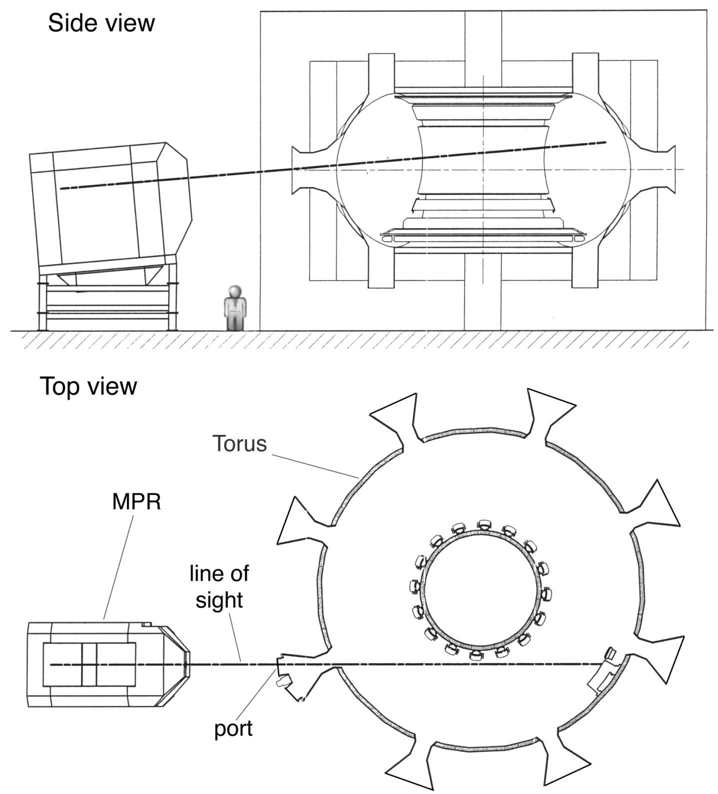

3.2. Neutron spectrometry: MPRu

MPRu main features:

- Absolute calibration
- High immunity to background

  14-MeV n in DT: S/B > 20000

  2.5-MeV n in DD: S/B > 10
- 2.5% resolution @ 14 MeV
- flux efficiency ~ 10^{-4} cm^2
- DAQ: count-rate >> MHz

Ohmic and ICRF heating plasmas

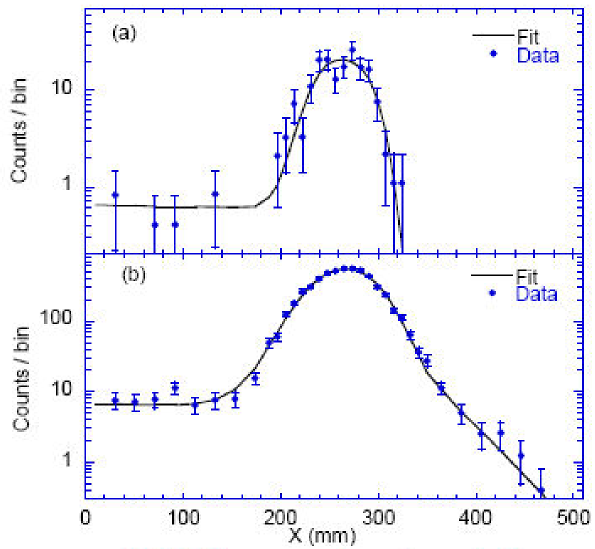

MPR histogram data from JET discharge 41759.

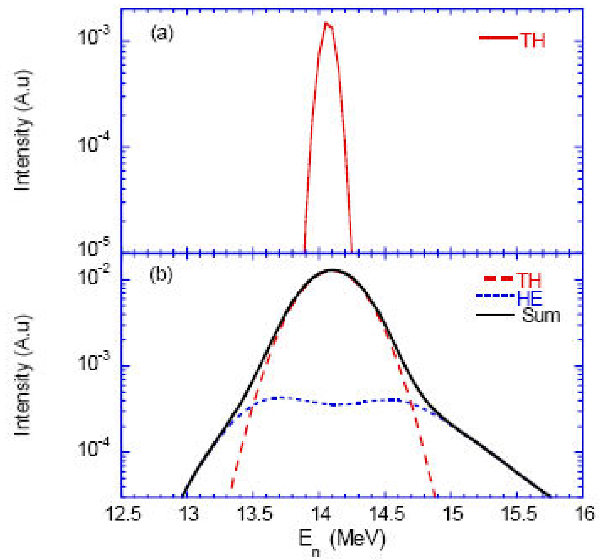

Spectral components from fit to MPR data (#41759)

(a) Ohmic phase – thermal Ti extracted
(b) RF phase – isotropic, anisotropic HE components

Confined α-particle diagnostics

4.1. Neutral Particle Analysers

The NPA measures the line integrated energy distribution function and fluxes.

Neutrals are generated via CX processes with bulk and impurity ions.

Carbon foils (300 Å) re-ionize the neutrals.

Acceleration provide boost to increase detection efficiency of low energy neutrals and to increase signal to noise ratio.

Momentum separation via B field
Mass separation via E field.

CsI(Tl) scintillator detectors coupled to PMT provide the signals for each individual neutral detected.

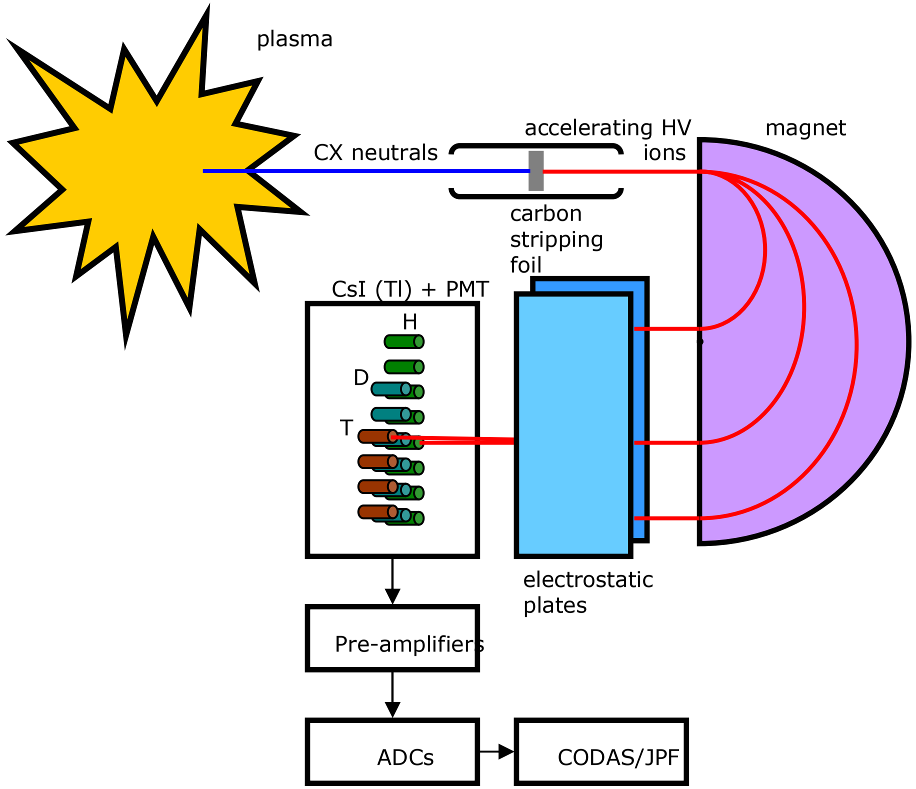

Si-detectors are installed to separate D and α's

Confined α-particle diagnostics

4.1. Neutral Particle Analysers: vertical view

R = 3.07 m

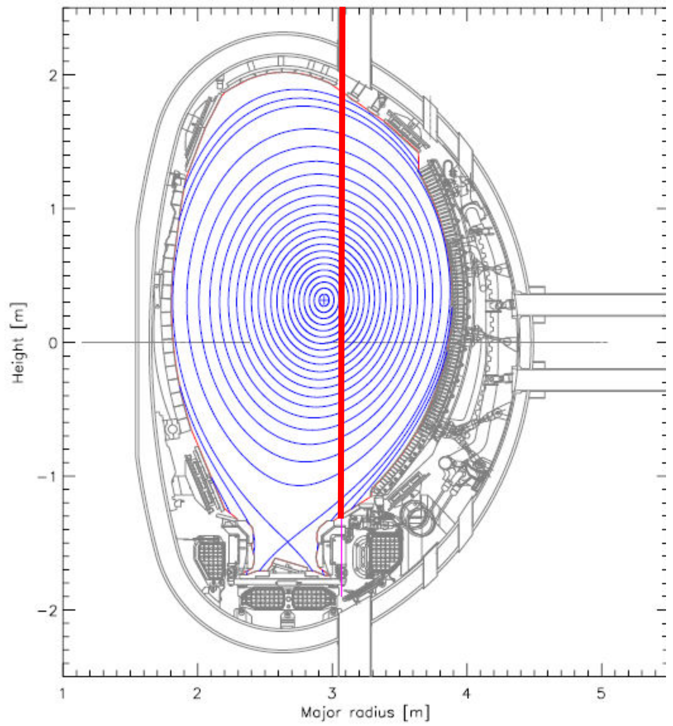

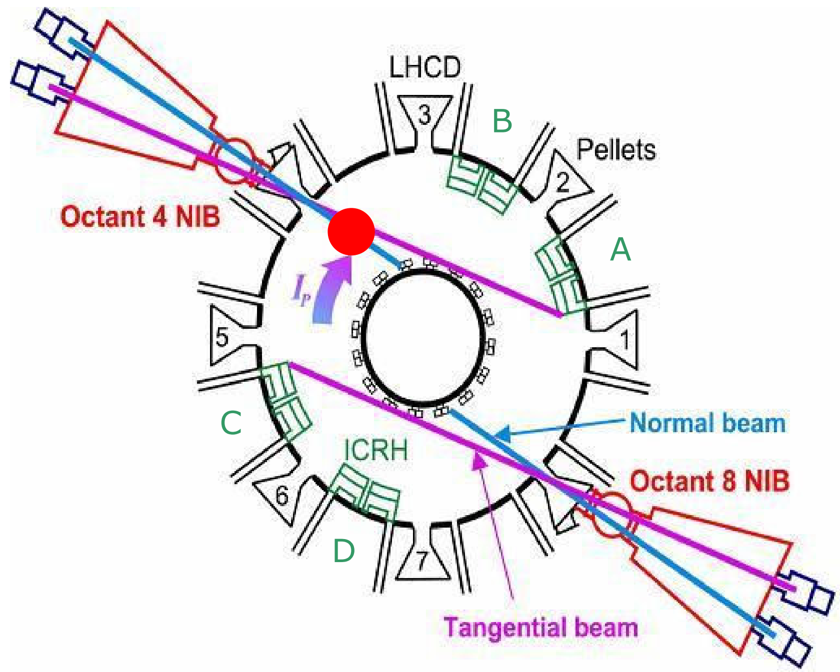

High-energy NPA measures the energy distribution function of neutral H, D, T, ^{3}He and ^{4}He in the energy range 0.3 – 4 MeV.

Confined α-particle diagnostics

4.1. Neutral Particle Analysers: horizontal view

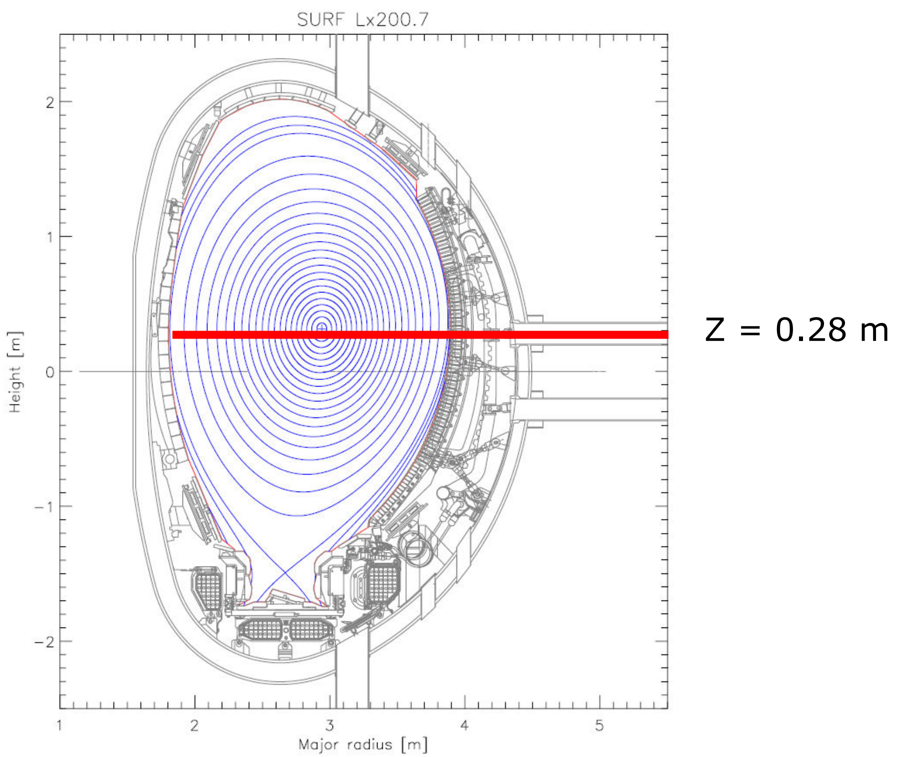

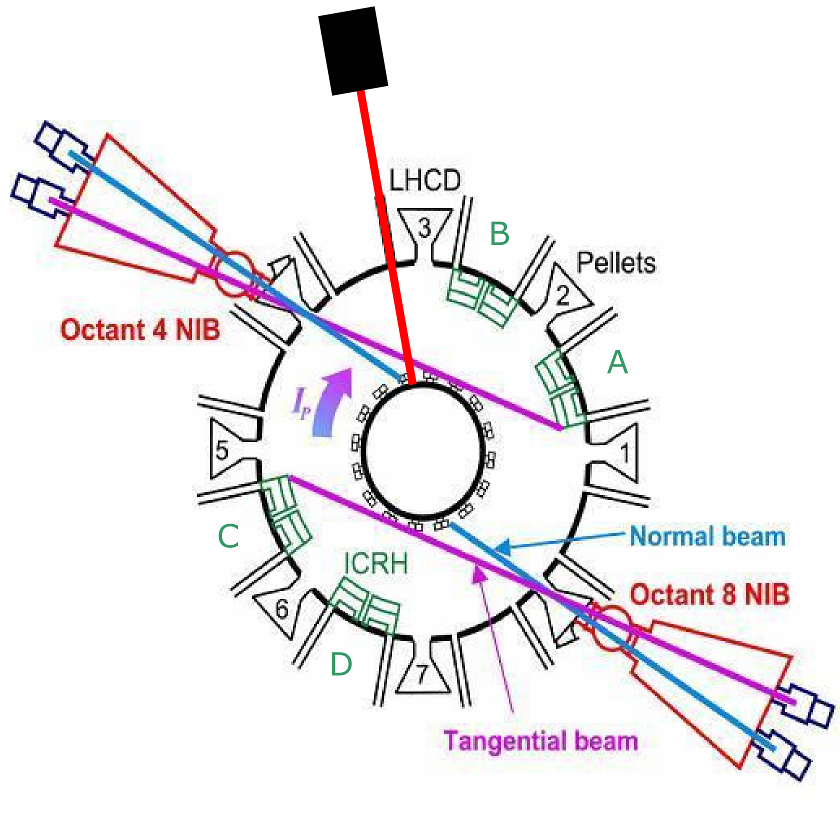

Low-energy NPA measures simultaneously the energy distribution function of neutral H, D and T in the energy range 5 – 740 keV.

Confined α-particle diagnostics

4.1. Neutral Particle Analysers: measurements

Effect of ICRH power in HE-NPA

ICRH with 42 MHz @ 3, 4 and 6 MW (R_{res}= 2.9 m)

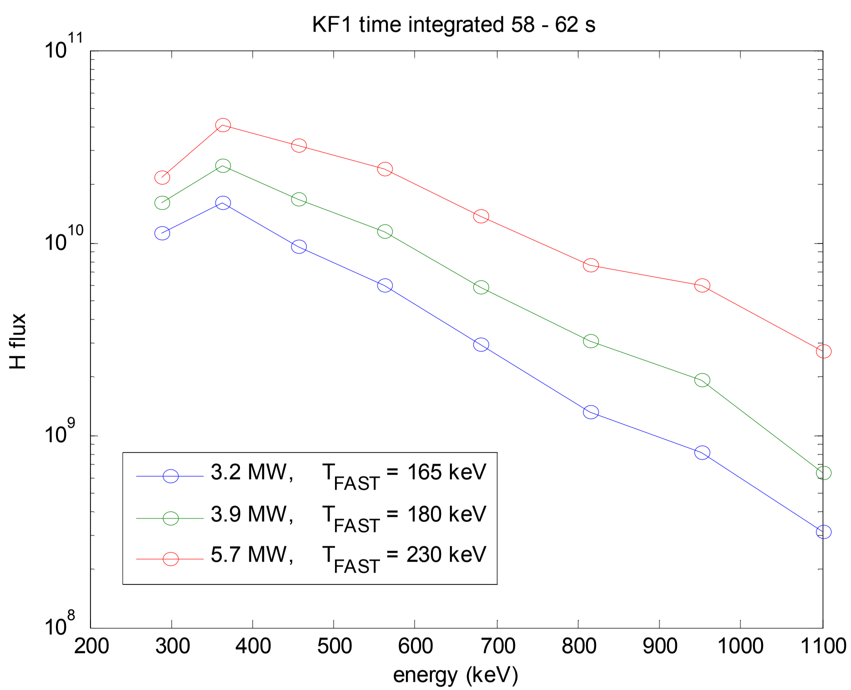

Auxiliary heating and neutral D-fluxes in LE-NPA

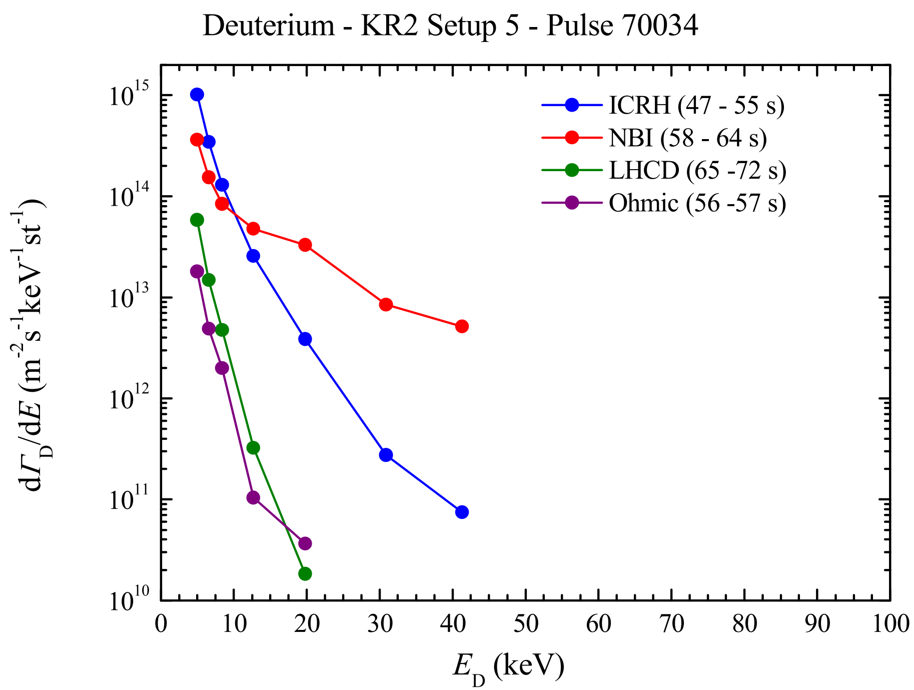

M. Cecconello

Confined α-particle diagnostics

4.1. Neutral Particle Analysers: measurements

Measurements of tritons in DD-plasmas with HE-NPA

The time evolution of T^0 fluxes and T-source during NBI heating

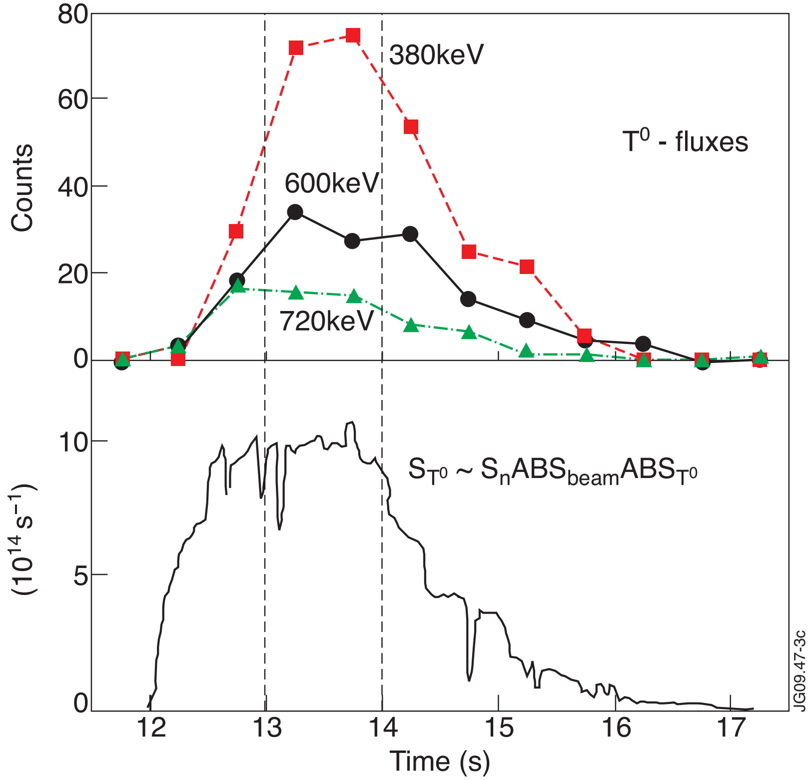

The charge-exchange energy spectrum T^0 atoms for the time 13s-14s

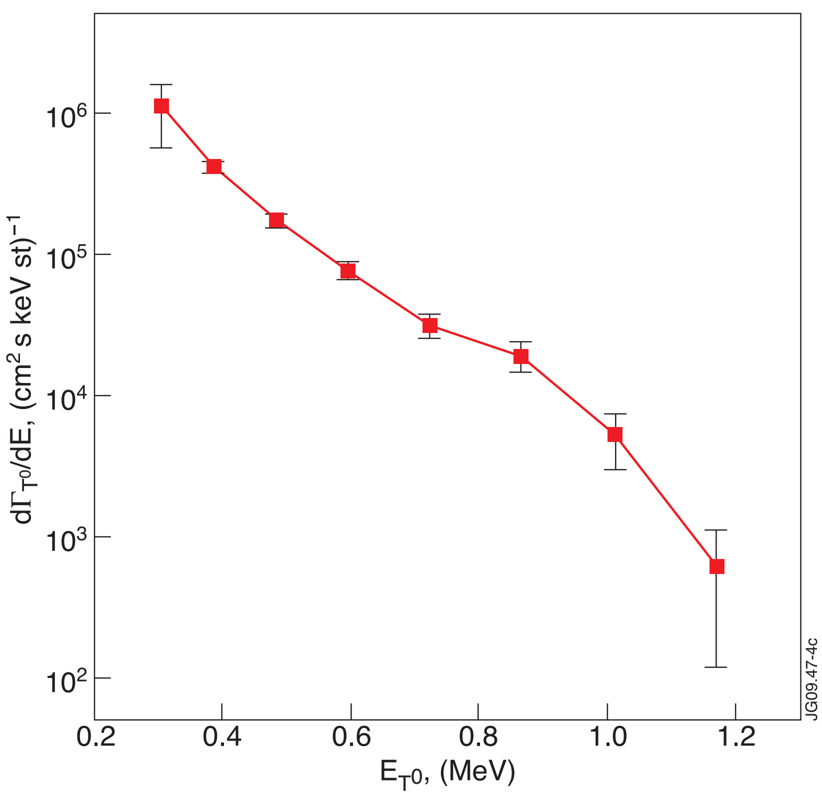

Confined α-particle diagnostics

4.2. Gamma-ray diagnostics

$^{9}Be(\alpha,n\gamma)^{12}C$ reaction

$^{9}Be + \alpha \rightarrow {}^{13}C^{*} \xrightarrow{n} {}^{12}C^{*} \xrightarrow{\gamma} {}^{12}C$

The nuclear reaction between fast α and ^{9}Be impurity leads to:

- Excitation of high-energy levels in $^{13}C^{*}$ nucleus
- De-excitation by emitting neutrons with population of the low-lying levels in $^{12}C^{*}$
- Further de-excitation by γ3.21 MeV and γ4.44 MeV to the ground state of ^{12}C nucleus:
  - γ4.44 MeV (E_{level} =4.44 MeV) are produced by α's with E_{α} > 1.7 MeV
  - γ3.21 MeV (E_{level} =7.65 MeV) are produced by α's with E_{α} > 4 MeV

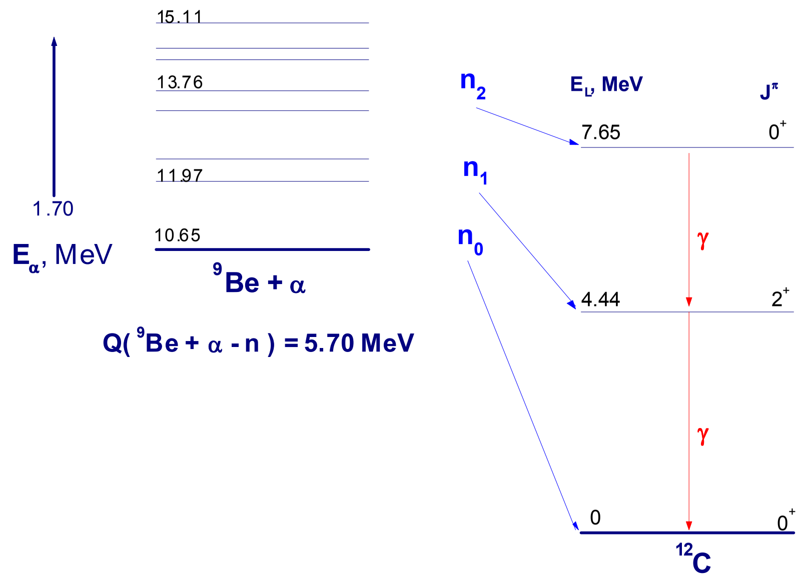

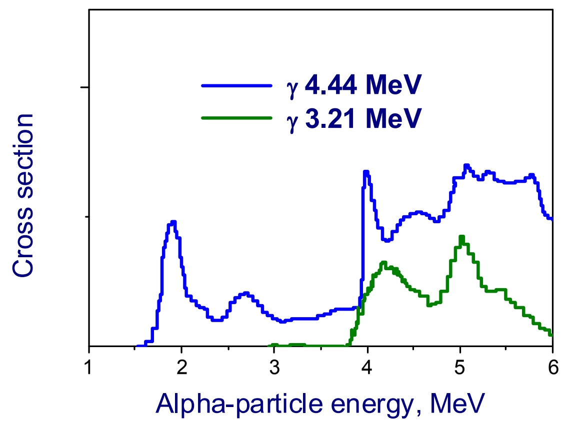

Confined α-particle diagnostics

4.2. Gamma-ray diagnostics: spectrometry

γ-rays interact with detector material

Photo-electric absorption | Compton scattering | e^-e^+ - pair production

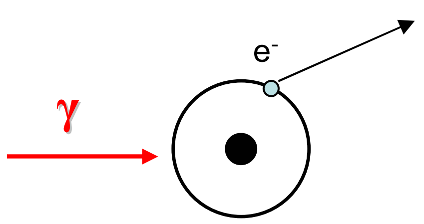

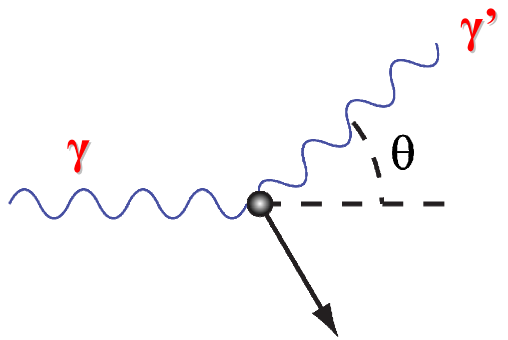

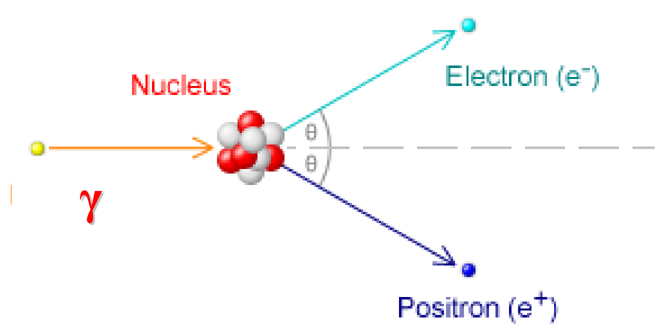

$$E_e = E_\gamma - E_b$$

$$\sigma \propto \frac{Z^{4\div5}}{E_\gamma^3}$$

$$E_\gamma^{'} = \frac{E_\gamma}{1 + \frac{E_\gamma}{m_0c^2}(1-\cos\theta)}$$

$$E_\gamma - 2m_0c^2 = E_{e^-} + E_{e^+}$$

$$E_\gamma^{min} > 2m_0c^2 = 1022\ keV$$

γ-detector → data acquisition system → memory → analysis

Confined α-particle diagnostics

4.2. Gamma-ray diagnostics: JET spectrometers

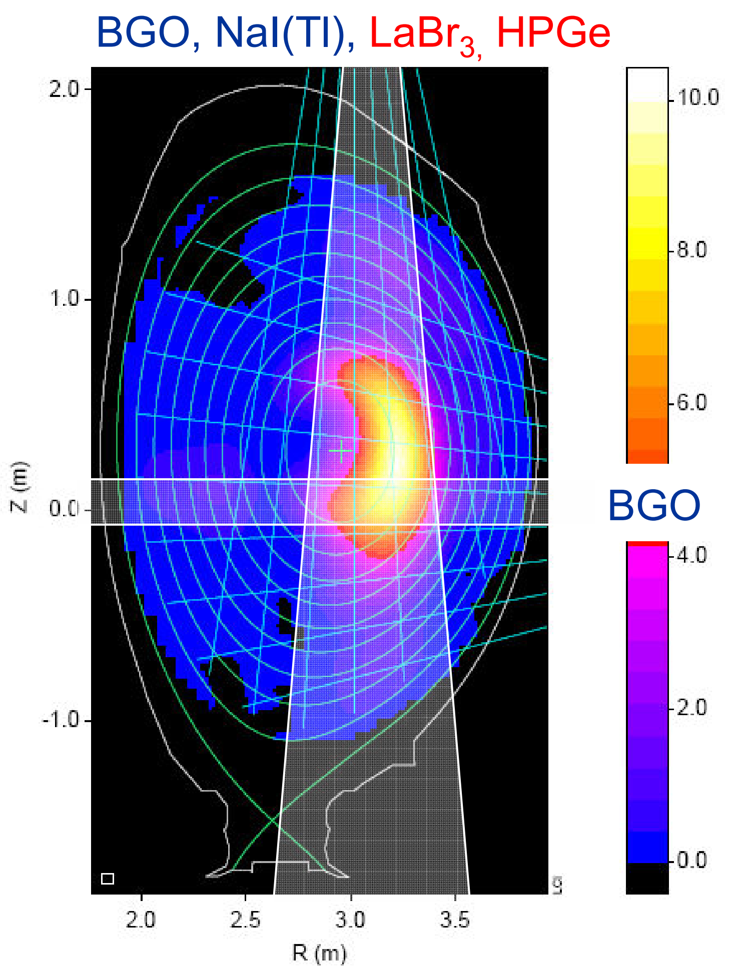

NaI(Tl): energy resolution, $\Delta E/E \approx 8\%$
Decay times - < 250 ns
Digital Data Acquisition system allows up to 1 MHz Pulse Height Analysis

$LaBr_3$ (or BrilLanCe): $\Delta E/E \approx 3\%$,
Decay times - < 20 ns
DAQ up to 5 MHz PHA

HPGe: $\Delta E/E \approx 0.3\%$ - the Doppler broadening of γ-lines can be measured!
DAQ up to 0.5 MHz PHA

4.2. Gamma-ray diagnostics: JET spectrometers (2)

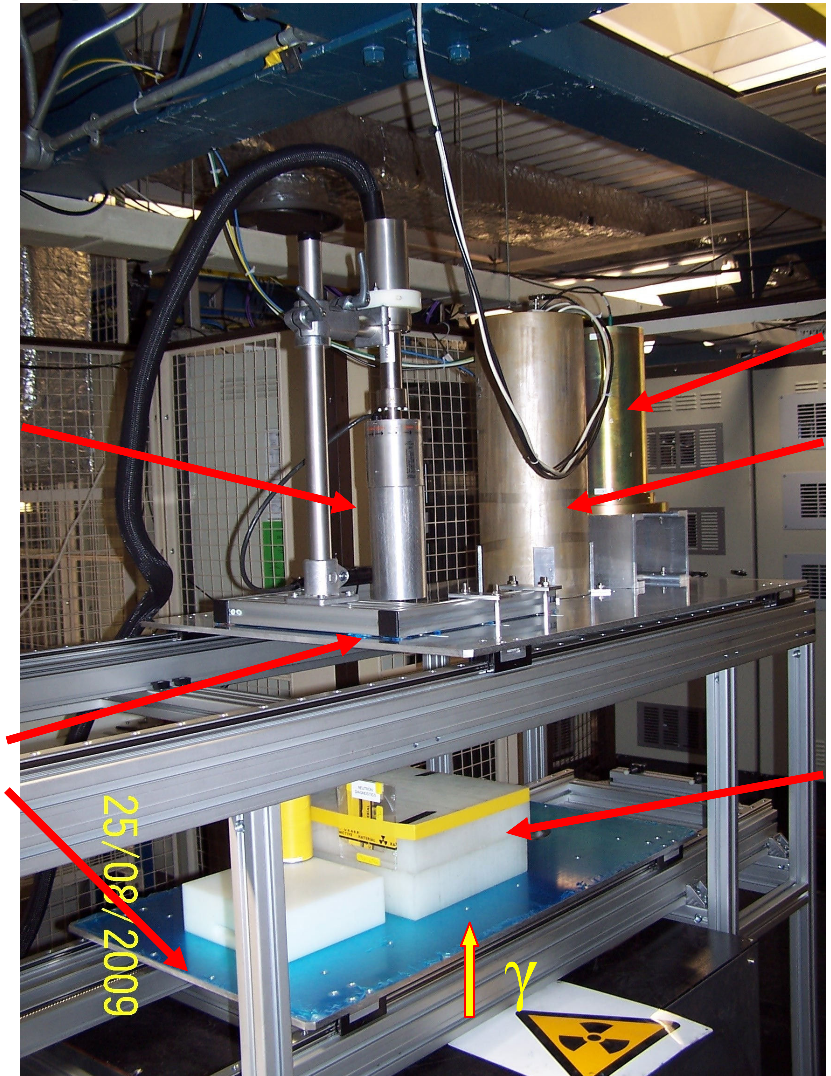

Confined α-particle diagnostics

4.2. Gamma-ray diagnostics: γ - spectra

γ-ray spectrum recorded in D(^{3}He)-plasmas

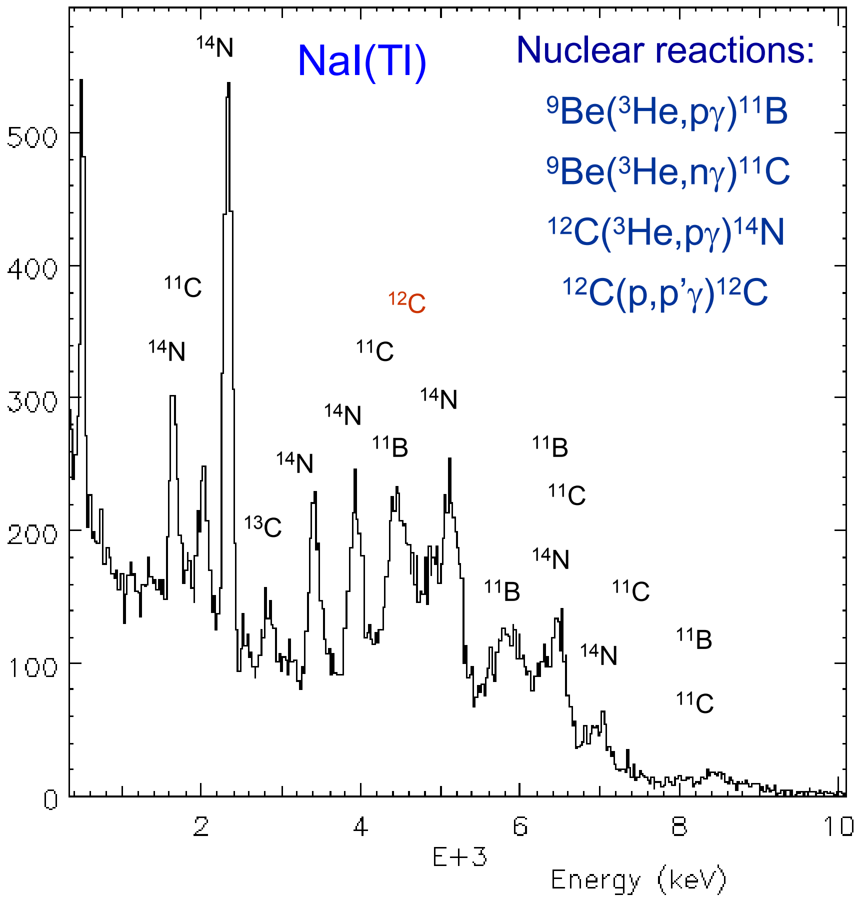

γ-ray spectra recorded in α-particle simulation experiment:

^{4}He- and D-ions accelerated in MeV-energy range with 3rd harmonic ICRF

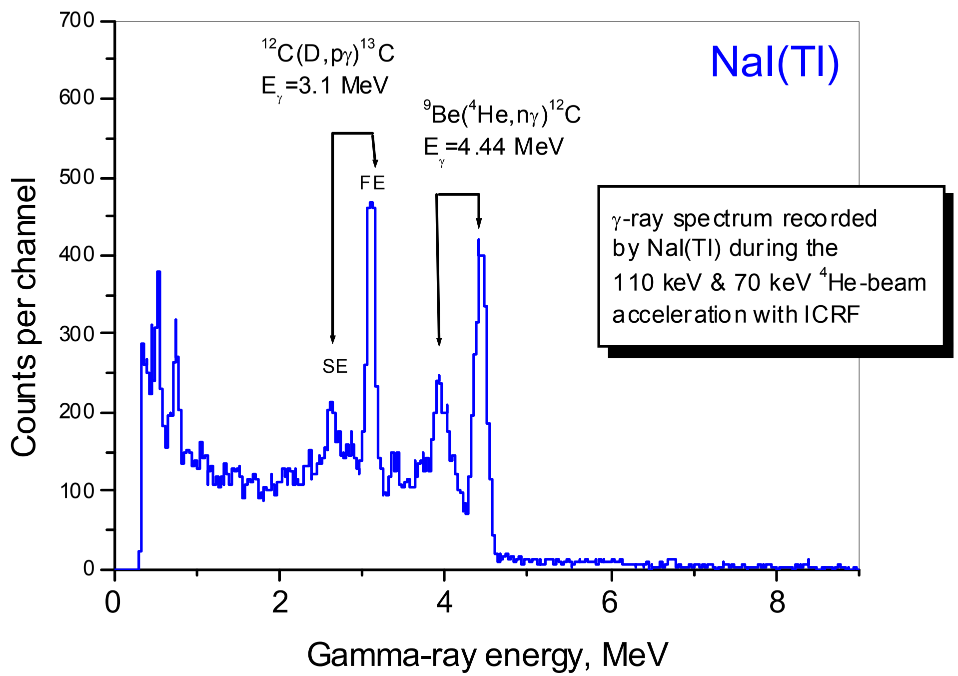

Confined α-particle diagnostics

4.2. Gamma-ray diagnostics: γ – spectra (2)

γ-ray spectrum recorded with HpGe-detector

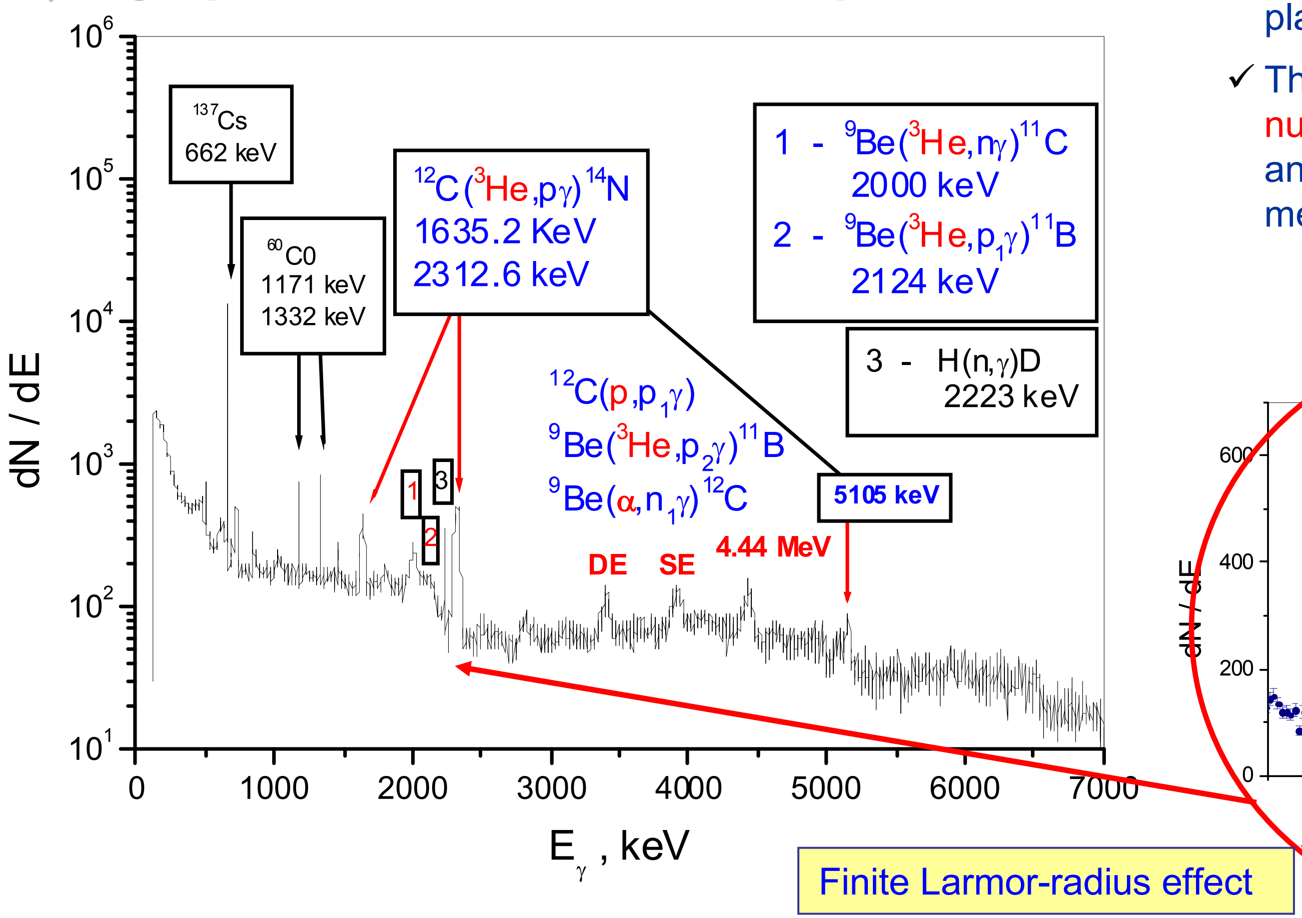

- ✓ ³He-minority ions was accelerated by ICRF in the DD-plasma
- ✓ The Doppler broadening due to nuclear reactions between ³He and C & Be impurities has been measured for $<T_{3He}>$.

$$E_\gamma \approx E_{\gamma 0} + E_{\gamma 0}(V_R/c)\cos\theta$$

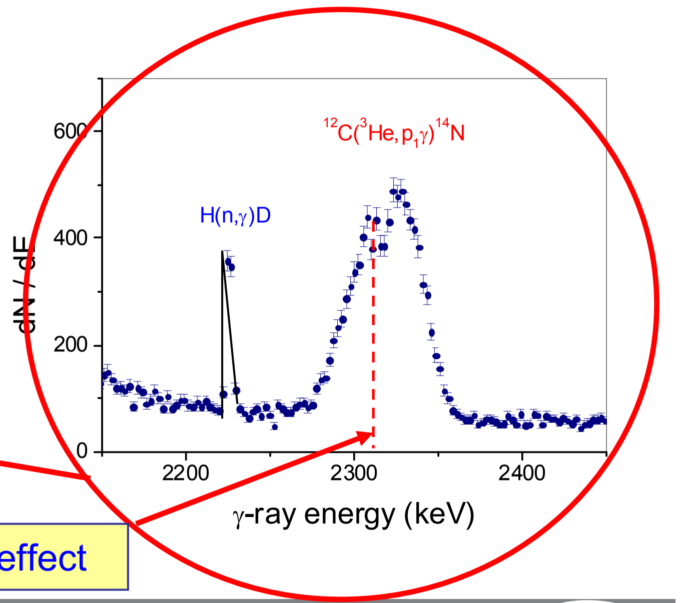

Confined α-particle diagnostics

4.2. Gamma-ray diagnostics: trace tritium experiments

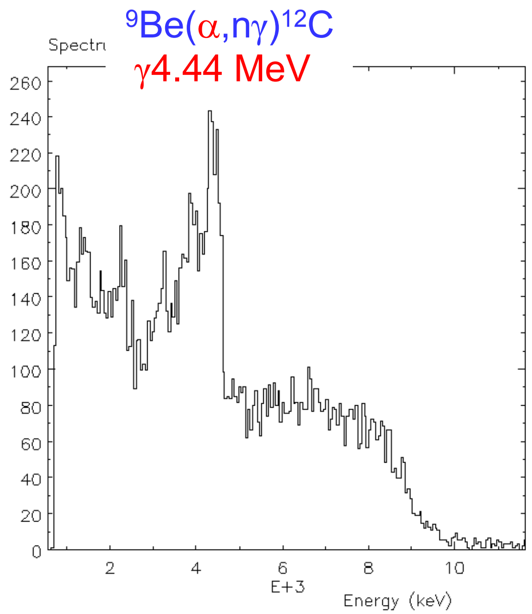

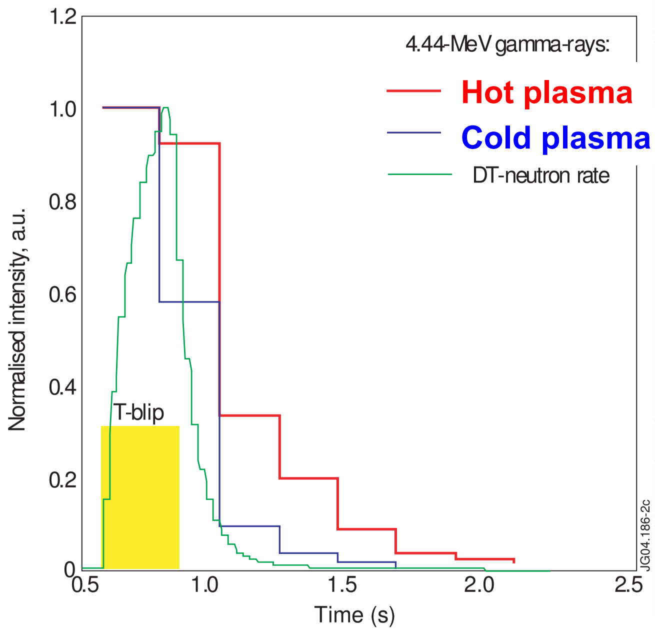

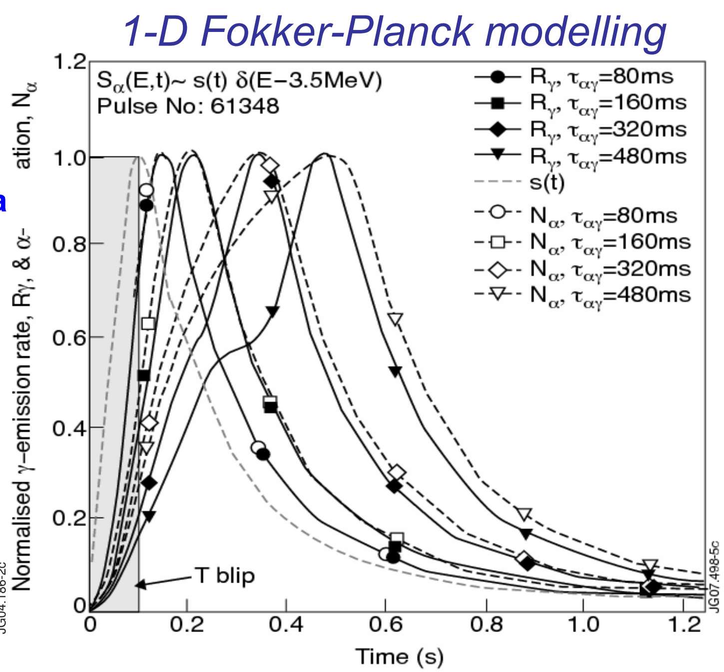

- γ-ray spectra recorded with BGO
- Relaxation of 4.44-MeV γ-ray intensity after the T-blip was measured.
- Time-resolution ~ 50 ms is required

Kiptily et al., PRL 93 (2004) 115001

- Relaxation of 4.44-MeV γ-ray emission and density of fast alphas (E>1.7MeV) depending on the value of Spitzer slowing-down time

Yavorskij et al NF **50** (2010) 025002

4.2. Gamma-ray diagnostics: ^{4}He acceleration experiments

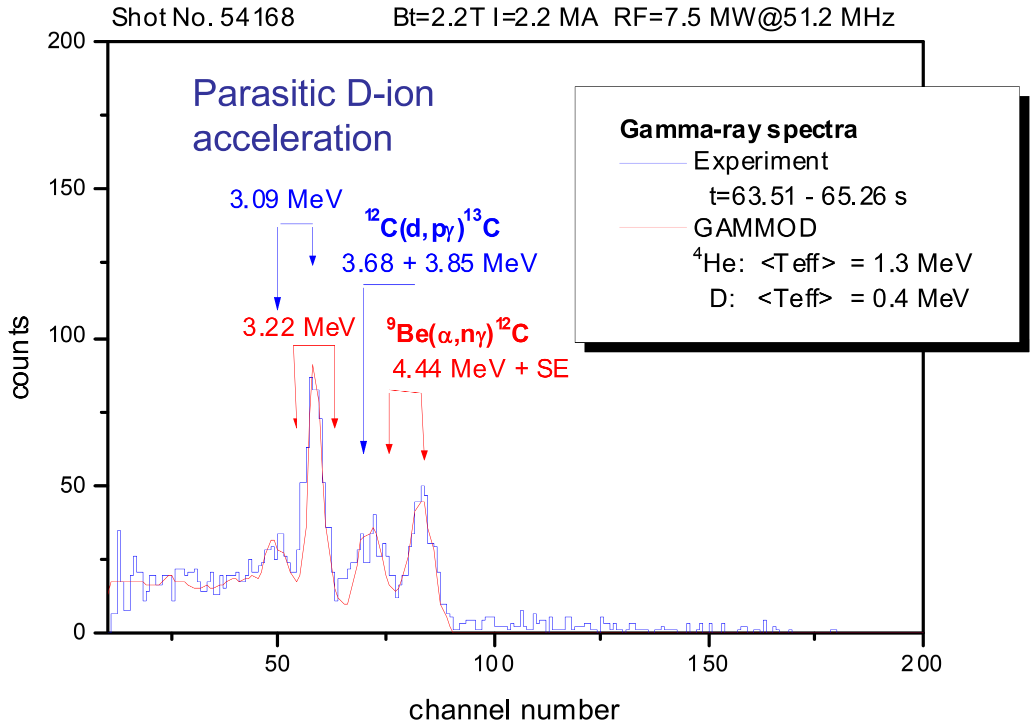

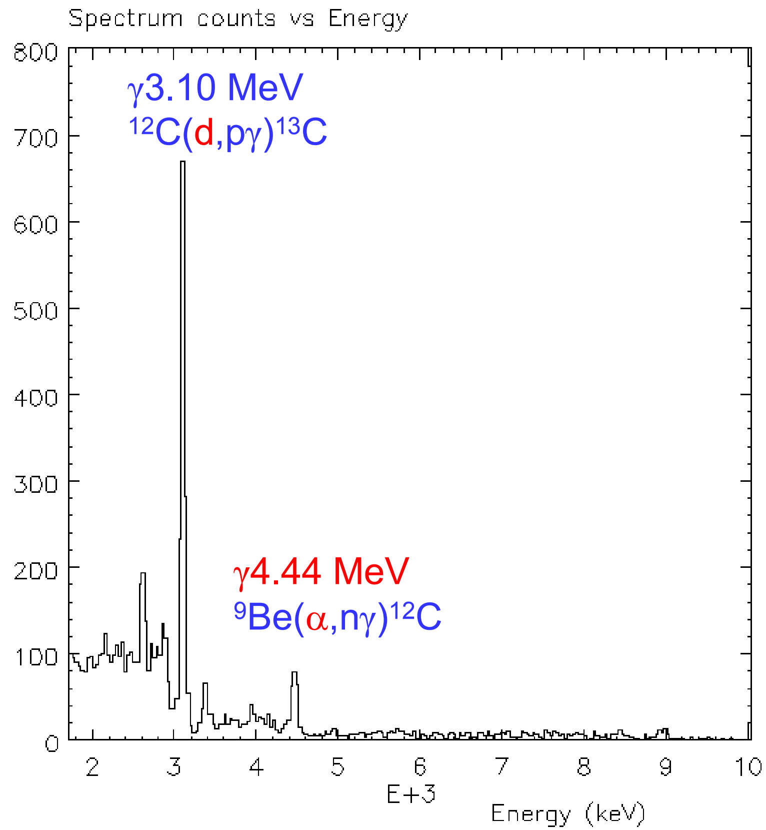

- γ-ray spectrum recorded with NaI(Tl)
- GAMMOD: modelled spectrum allows assess tail temperature and relative fast-ion density Kiptily et al NF **42** (2002) 999

- γ-ray spectrum recorded with $LaBr_3$
- High resolution spectrometry will provide more reliable data

M. Tardocchi et al HTPD-2010

Confined α-particle diagnostics

4.2. Gamma-ray diagnostics: ^{4}He acceleration experiments

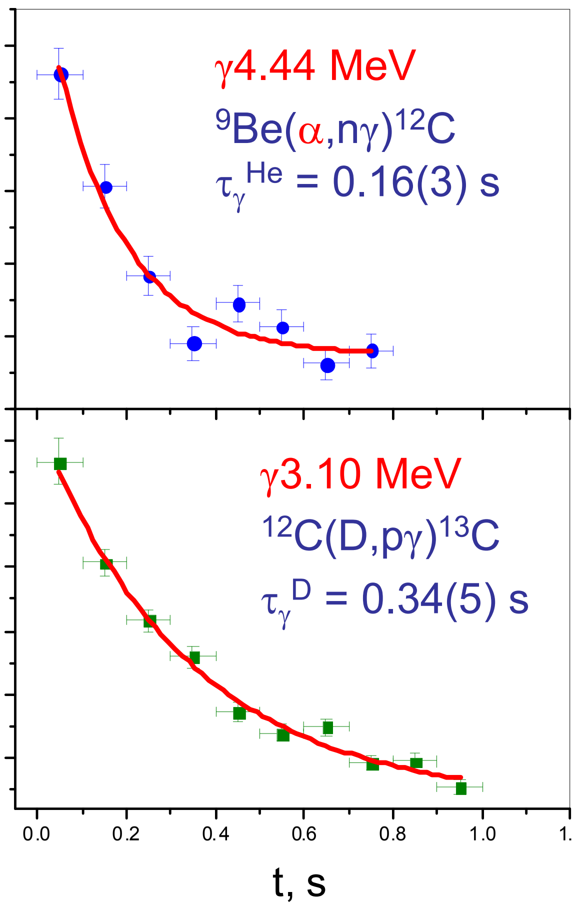

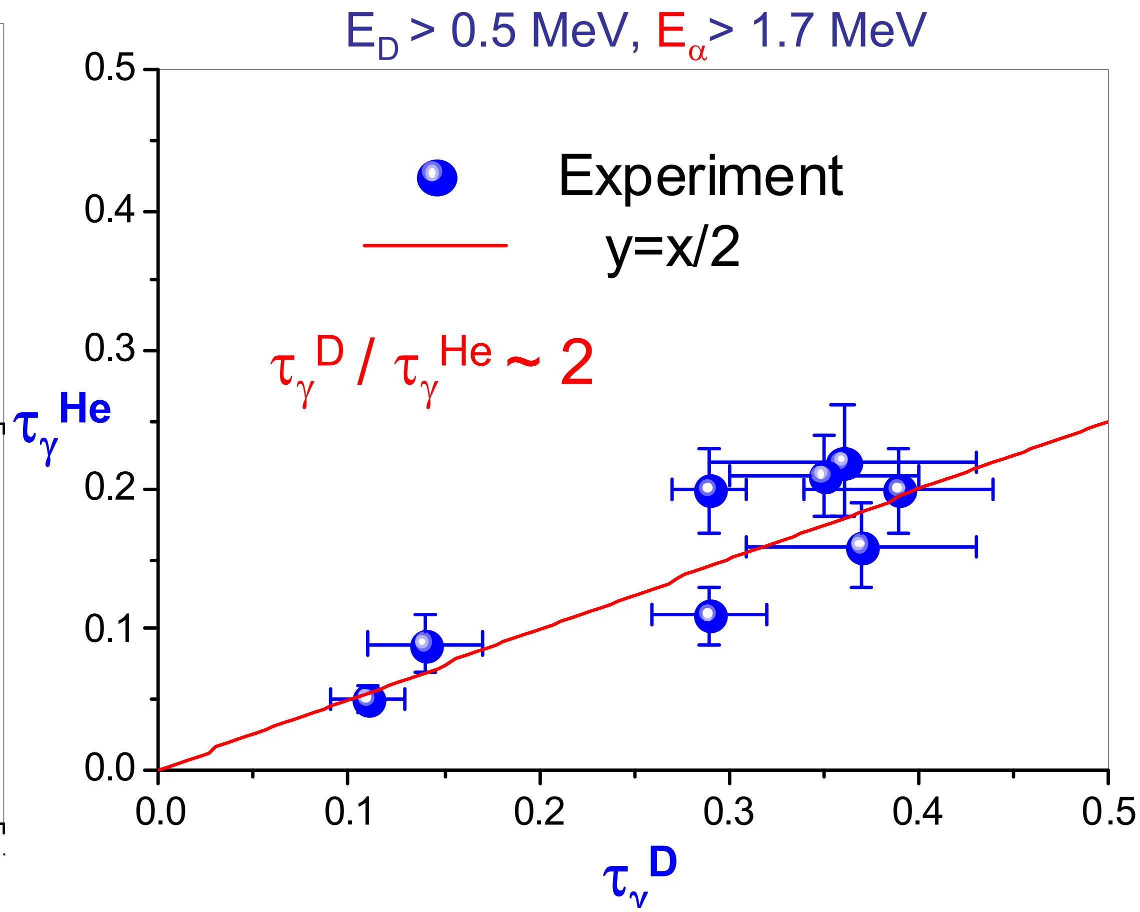

Consistent with theory: $\tau_s \propto A / Z^2$

Confined α-particle diagnostics

4.2. Gamma-ray diagnostics: ^{4}He acceleration experiments

monotonic q-profile

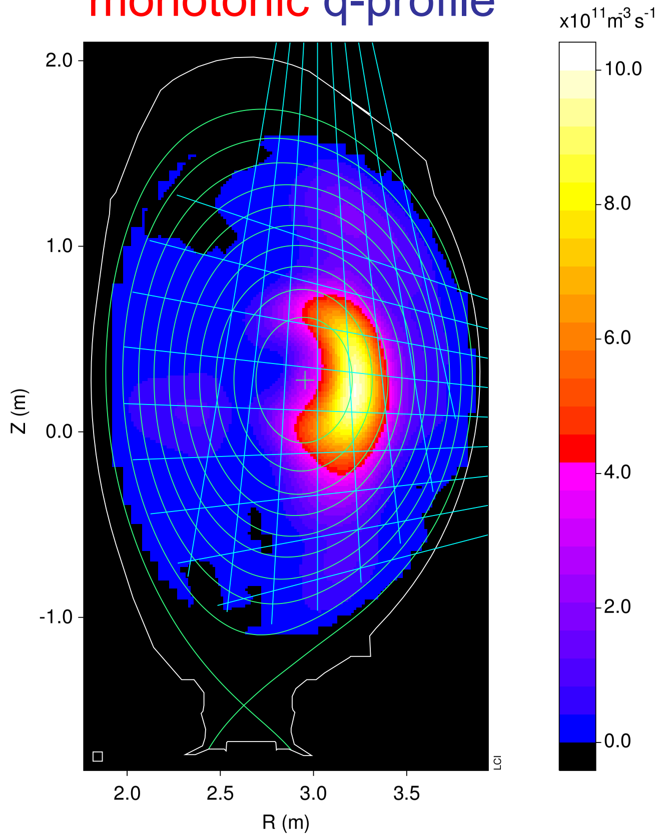

non-monotonic q-profile

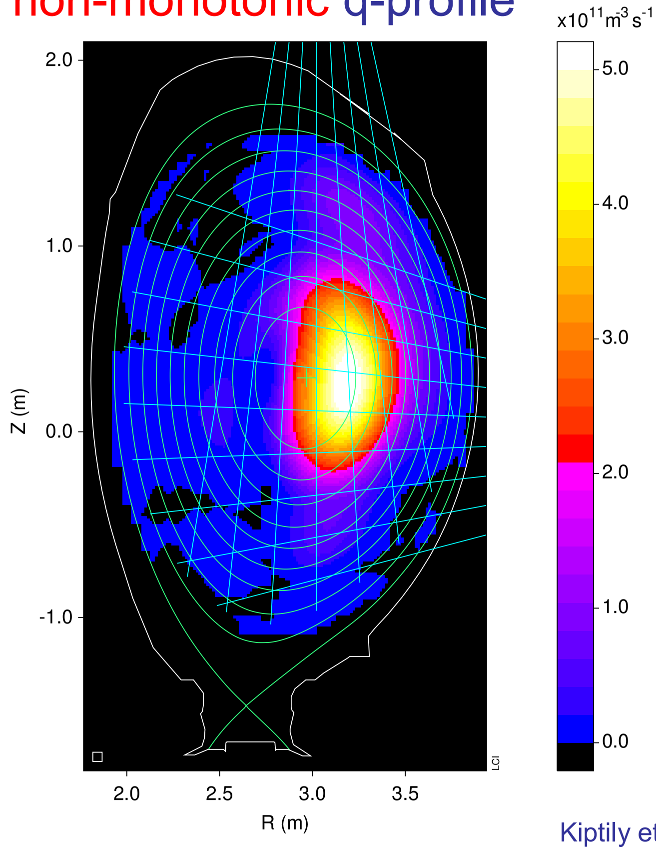

Kiptily et al NF **45** (2005) L21

Tomographic reconstructions of profiles measured in different q-profile phases of the optimised shear plasma discharge. The monotonic q-profile was settled down after sawtooth crash.

Confined α-particle diagnostics

4.2. Gamma-ray diagnostics: modelling for ITER

Gamma-ray emission from the D(t,γ)^{5}He reaction (3.5-MeV alpha-source) and ^{9}Be(α,nγ)^{12}C reaction (~2-MeV alphas) could be used for monitoring DT-plasma performance

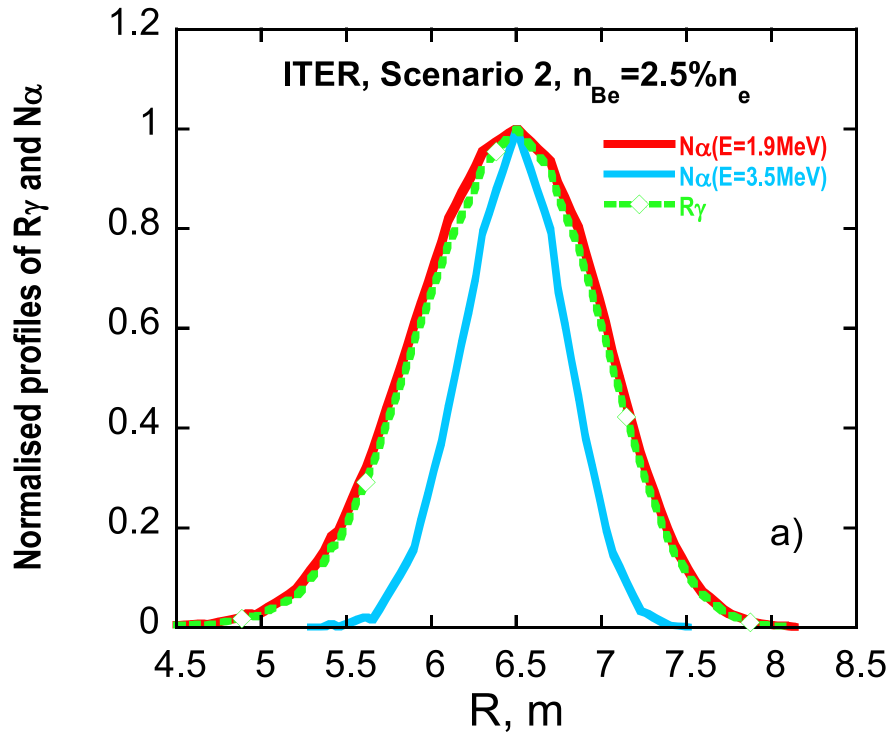

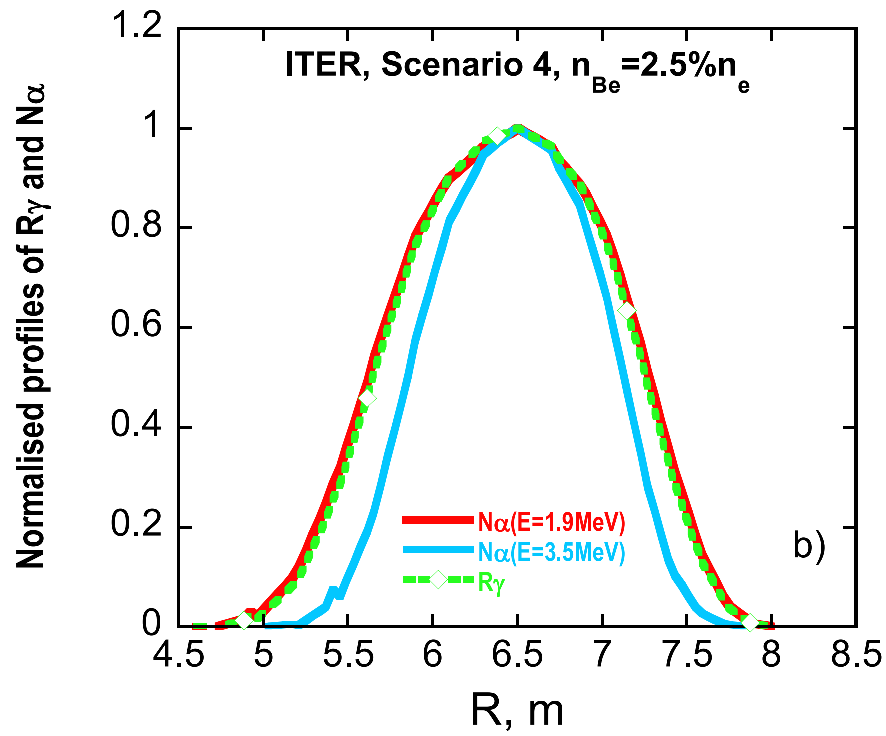

V. Yavorskij at al 35th EPS, P1.087, Greece, 2008

CCFE CULHAM CENTRE FOR FUSION ENERGY

Confined α-particle diagnostics

4.2. Gamma-ray diagnostics: modelling for ITER

Line integrated γ-ray emission from the diagnostic reactions for α-particle and D-beam ions measurements calculated for the Radial Camera (n_{Be}=2.5%)

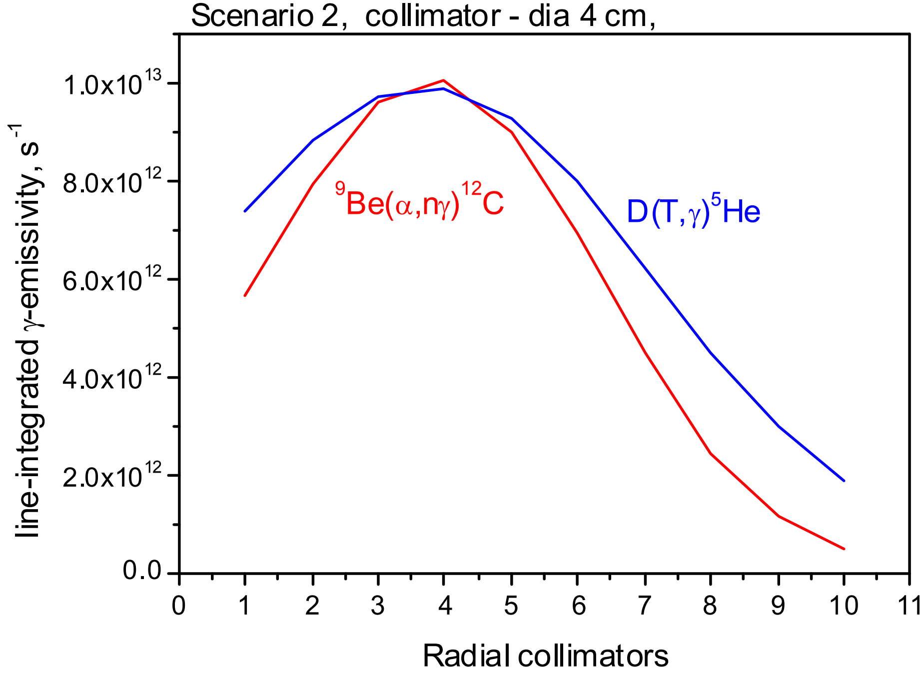

It is feasible for trace-tritium or fully tritium plasmas

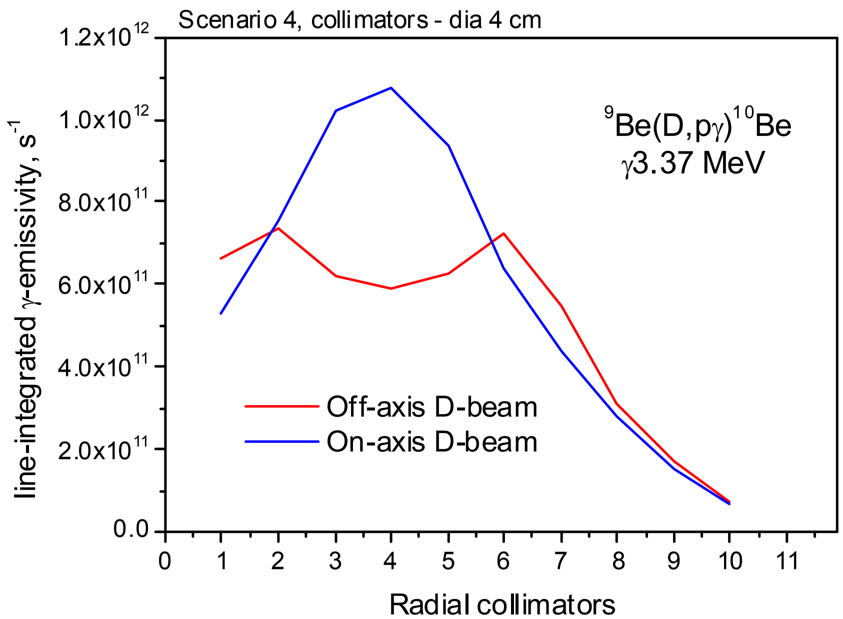

Modelling shows that the reaction rates are sufficiently high for implementing of the techniques on ITER

Final Report on the EFDA task TW6-TPDS-DIADEV, 2007

Confined α-particle diagnostics

4.2. Gamma-ray diagnostics: modelling for ITER

SELFO modelled profiles of γ -ray emissivity due to $^{9}Be(^{3}He,p\gamma)^{11}B$

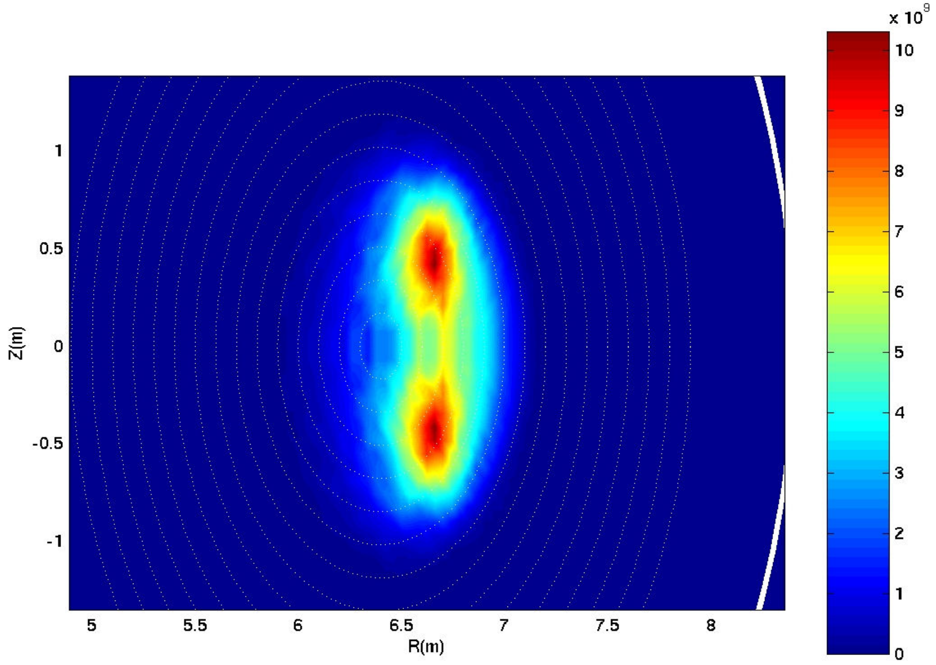

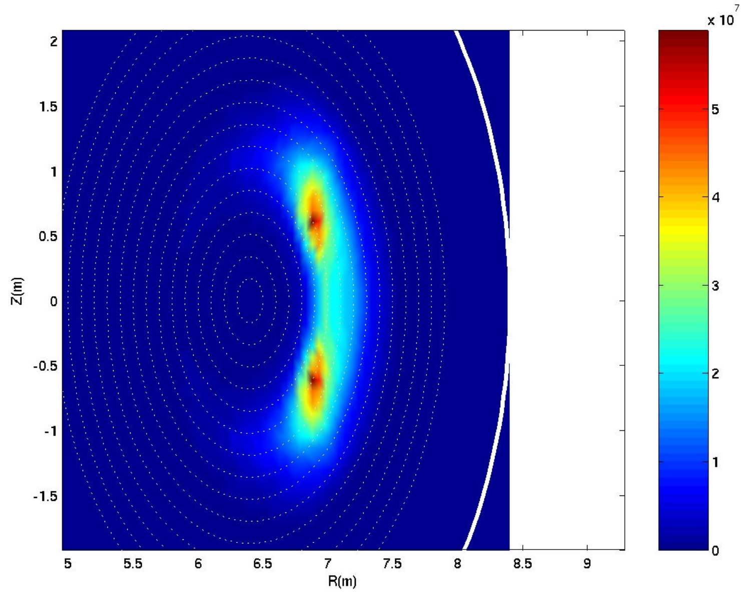

*R*eaction rate in 2nd scenario: standard H-mode,
$n_{He\text{-}3} / (n_D + n_T)$ = 1%, f_{ICRF} = 52MHz

The same, but f_{ICRF} = 50MHz.

The γ-ray rates are sufficiently strong to be measured

Final Report on the EFDA task TW6-TPDS-DIADEV, 2007

Confined α-particle diagnostics

4.2. Gamma-ray diagnostics: modelling for ITER

SELFO modelled profile of γ -ray emissivity due to $^{9}Be(t,n\gamma)^{11}B$

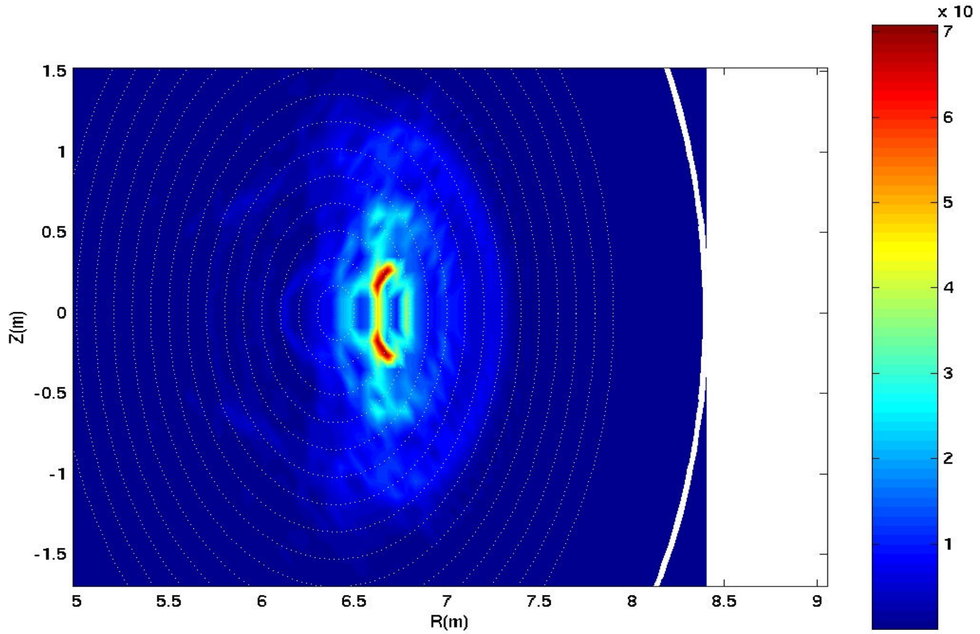

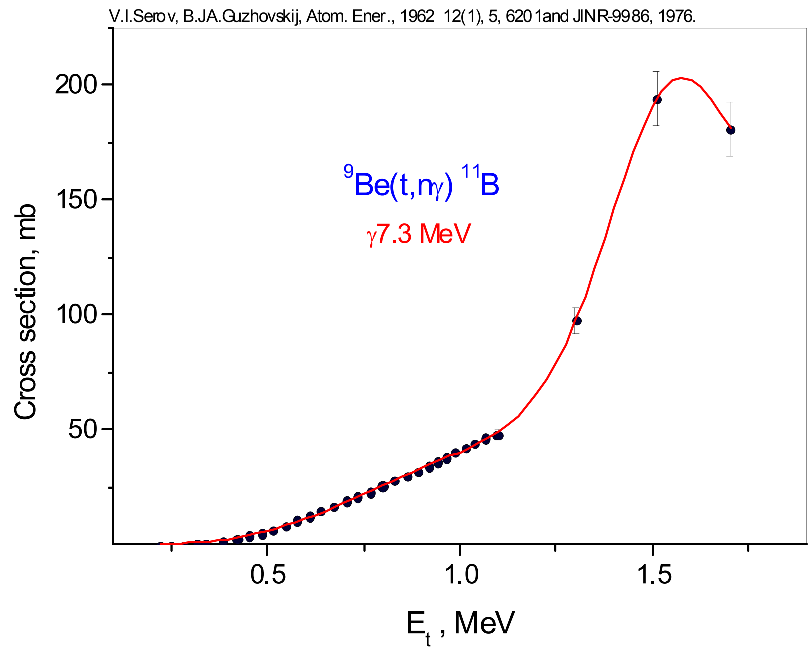

Reaction rate in 2nd scenario: standard H-mode, pure $\omega=2\omega_{cT}$ heating with central cyclotron resonance. The 7.3 MeV γ-ray rate is sufficiently strong to be measured.

Final Report on the EFDA task TW6-TPDS-DIADEV, 2007

4.2. Gamma-ray diagnostics: modelling for ITER

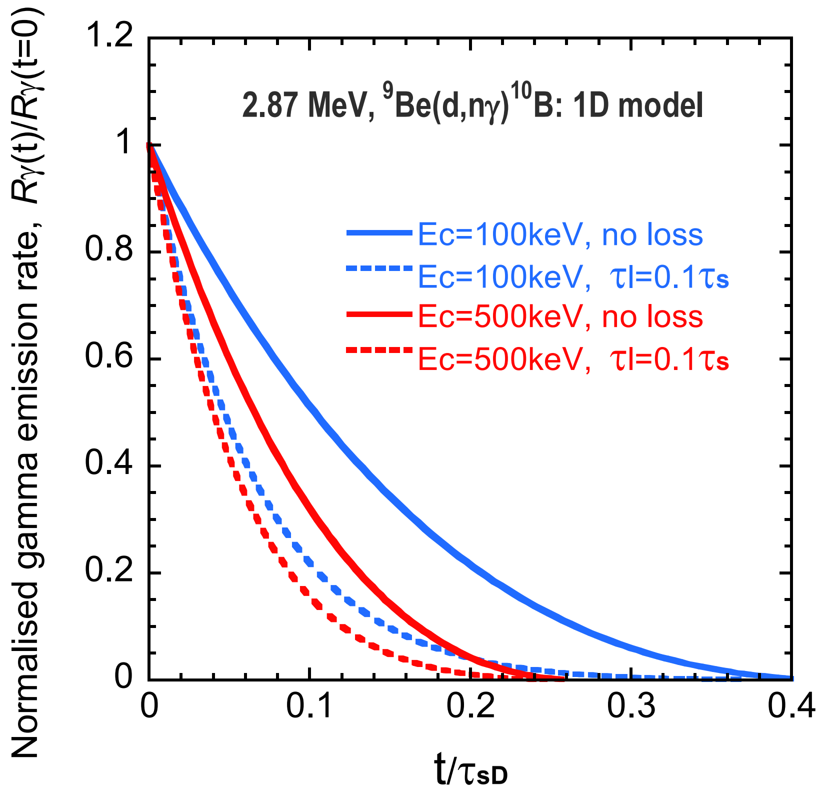

- 1-D Fokker-Planck modelling of 2.87-MeV γ-ray emissivity of $^{9}Be(D,n\gamma)^{10}B$
- Relaxation of 2.87 MeV γ-ray emission from nuclear reactions after NBI switch-off.
- Poor confinement associated with $\tau_{loss}<0.1\tau_s$ will significantly enhance the decay rates of γ-ray emission.
- γ-ray measurements with ~ 50ms time resolution are required for slowing-down and D-beam loss-rate assessments

$$R_\gamma(t>0) \propto \sqrt{E}\int_t^{\tau_{D\gamma}} d\tau\, \sigma_\gamma(E')\sqrt{E'}\exp\left(-\frac{\tau}{\tau_l}\right)\Bigg|_{E=E_0}, \quad E_0 = 1\,\text{MeV} \;\text{ and }\; E_c \sim 20Te$$

V. Yavorskij at al IAEA FEC, TH/P3-2, Geneva 2008

Confined α-particle diagnostics

4.2. Gamma-ray diagnostics: γ - camera for ITER (project)

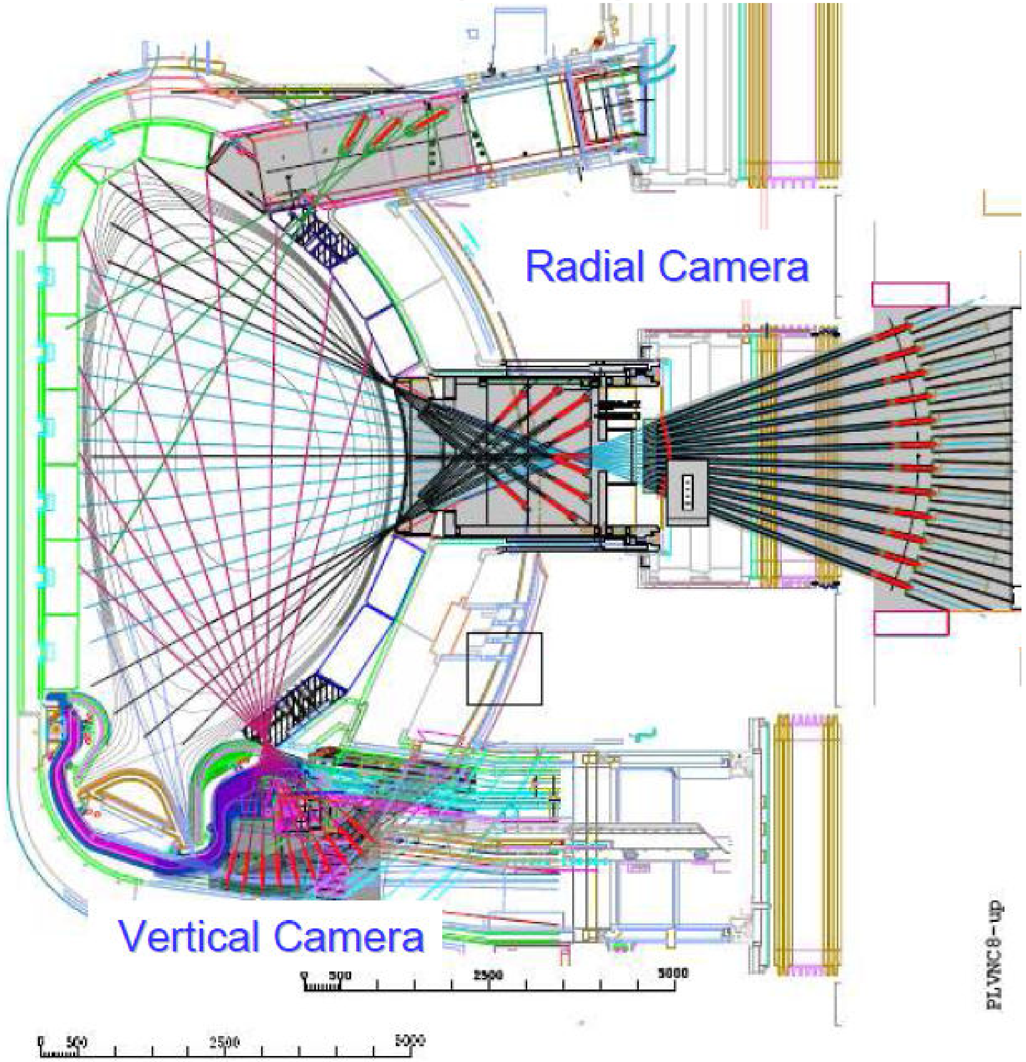

Radial camera for neutrons and gammas:

12 ex-vessel views (36 channels)

8 in-vessel views (port)

Vertical camera – in divertor (project)

γ-ray collimators should be equipped with neutron attenuators

^{6}LiH is proposed: high-efficient neutron attenuator, γ-ray transparent

1-m-long ^{6}LiH-attenuator:

10^{-10} (DD-neutrons) and

10^{-5} (DT-neutrons)

Attenuation range $10^{-1} \div 10^{-6}$ is required

Confined α-particle diagnostics

4.2. Gamma-ray diagnostics: neutron attenuation

Test of ^{6}LiH neutron attenuator on JET

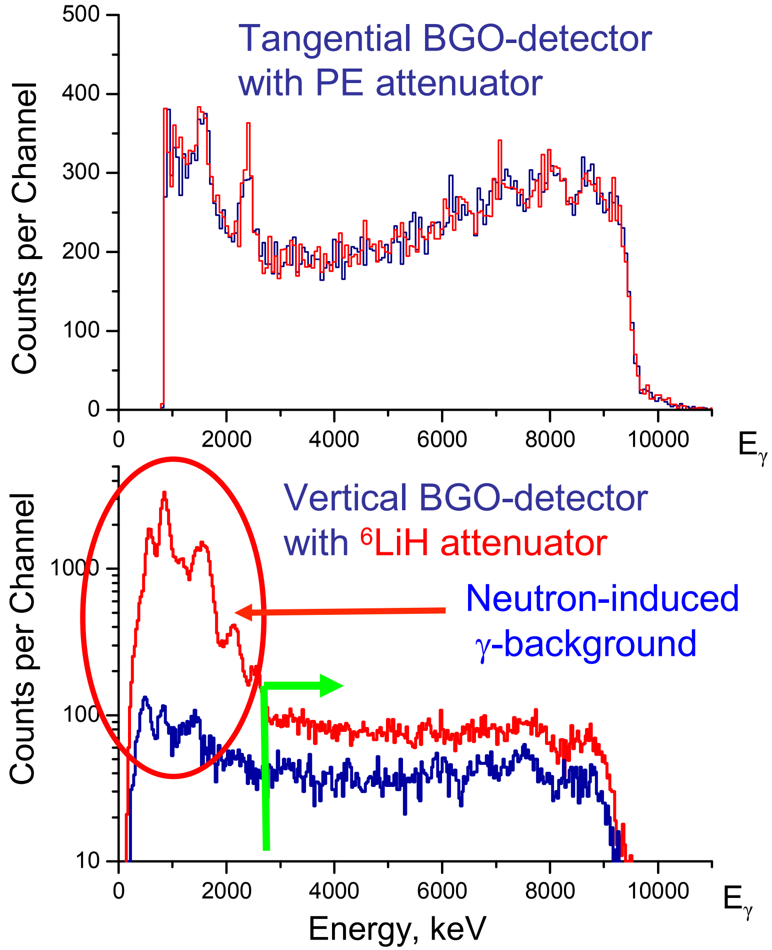

Chugunov et al., Instrum. and Exp Techniques **51** (2008) 166

<= Reference spectrum measurements

Neutron-induced gammas in the range E_γ<3 MeV (inelastic nuclear scattering in detector) suppressed with ^{6}LiH attenuator by a factor of ≈100

Gamma-rays with E_γ > 3 MeV suppressed with ^{6}LiH attenuator by a factor of ≈2

Escaped α-particle diagnostics

5.1. Scintillator probe: in JET

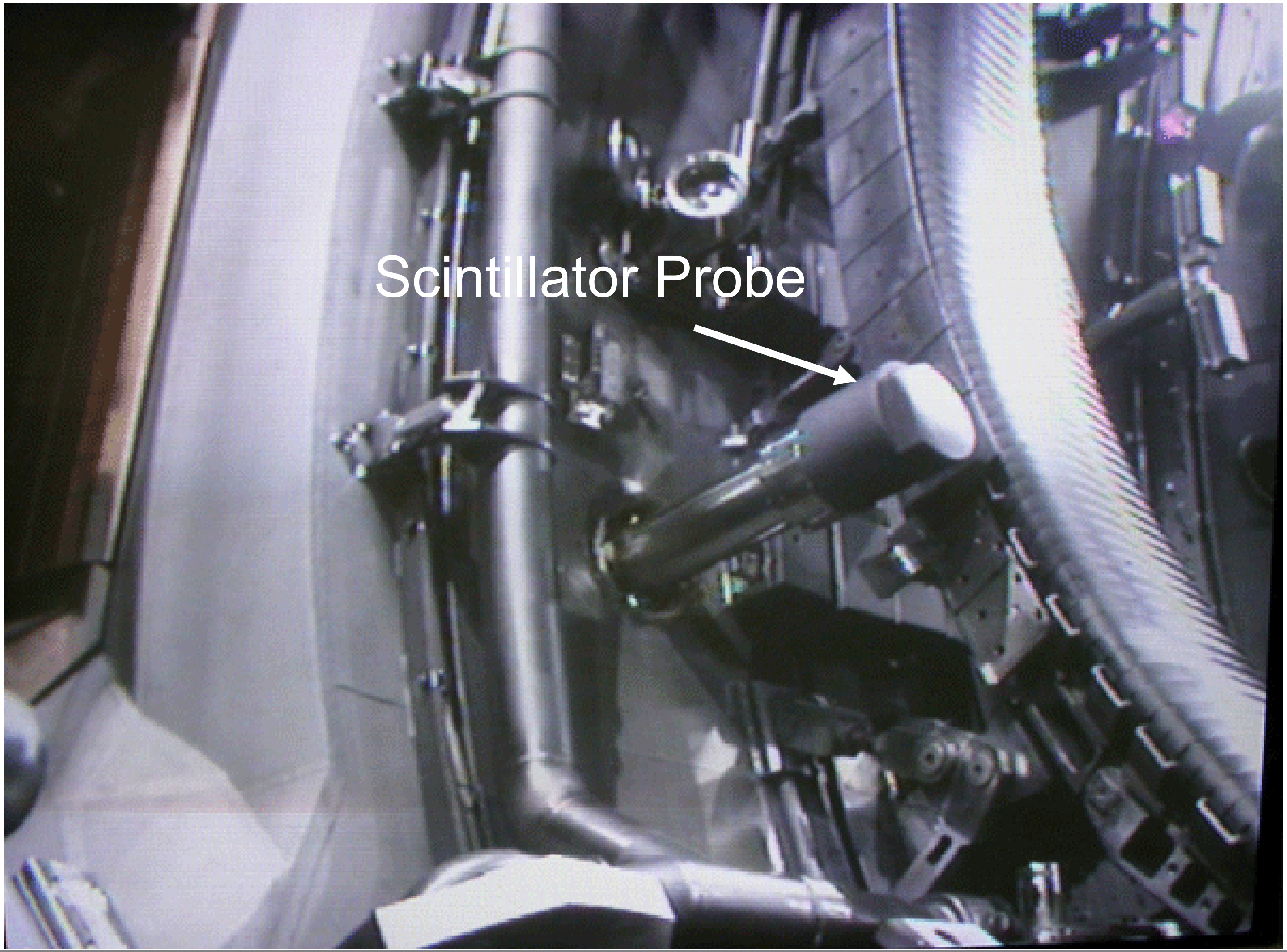

Escaped α-particle diagnostics

5.1. Scintillator probe: basic principle

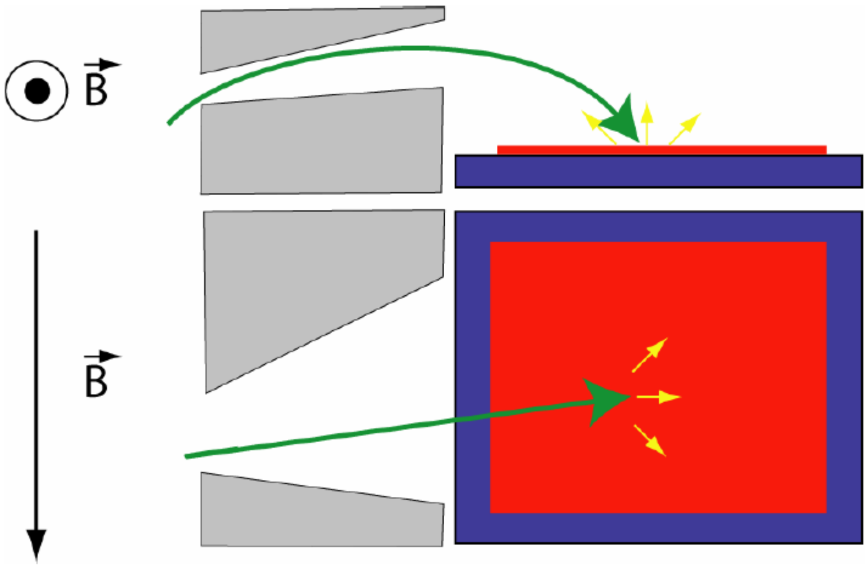

- Gyromotion of fast ions
- Particle selection by slits
- Light emission by scintillator

Gyro-radius $\rho \propto \frac{mV_\perp}{ZB}$

Pitch-angle $\theta = \cos^{-1}\frac{V_{II}}{V}$

Species	ρ(B=3T)
α(3.5 MeV)	9.0 cm
P(3.0 MeV)	8.3 cm
T(1.0 MeV)	8.3 cm
^{3}He(0.82 MeV)	3.8 cm

Escaped α-particle diagnostics

5.1. Scintillator probe: real orbit simulation

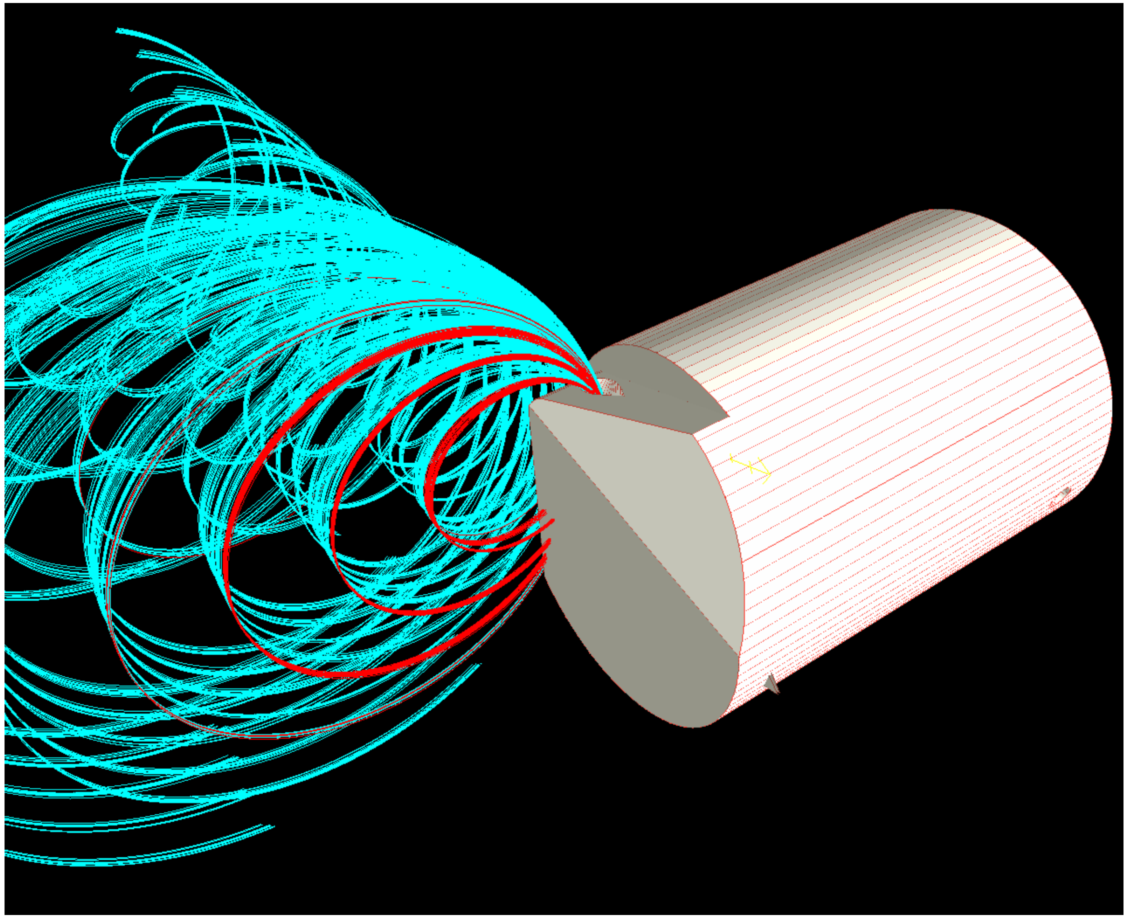

View along tube axis

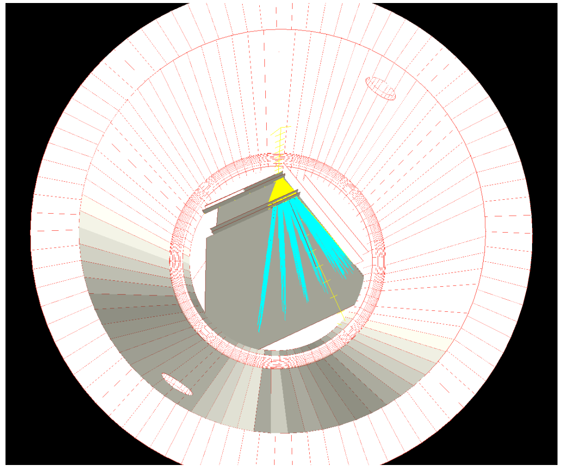

SP detects ions with

gyro-radius from *3 cm* to *14 cm*

pitch-angle from *35^0 to 85^0*

Escaped α-particle diagnostics

5.1. Scintillator probe: basic set-up

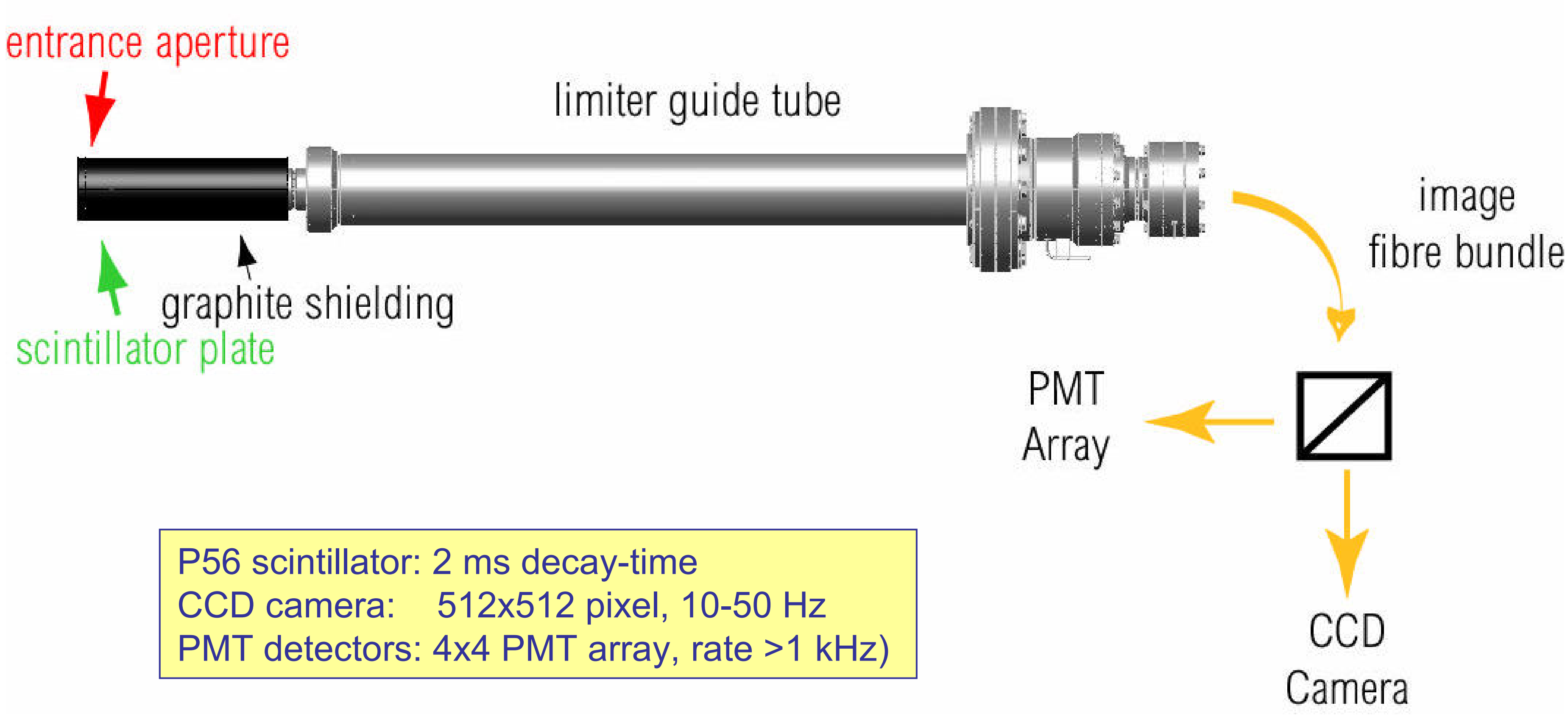

P56 scintillator: 2 ms decay-time
CCD camera: 512x512 pixel, 10-50 Hz
PMT detectors: 4x4 PMT array, rate >1 kHz)

Escaped α-particle diagnostics

5.1. Scintillator probe: measurements

Footprints of the lost D- and H-ions during "sawtooth crash"

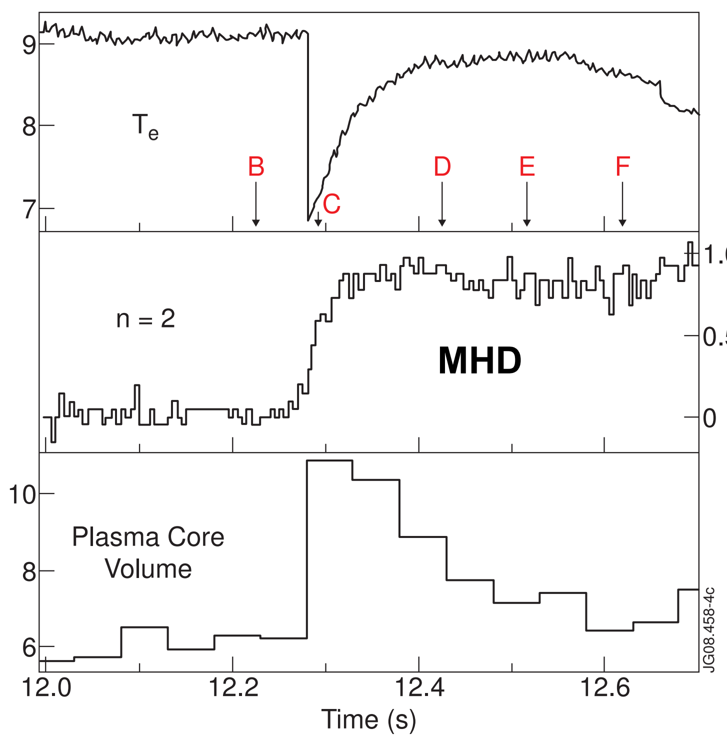

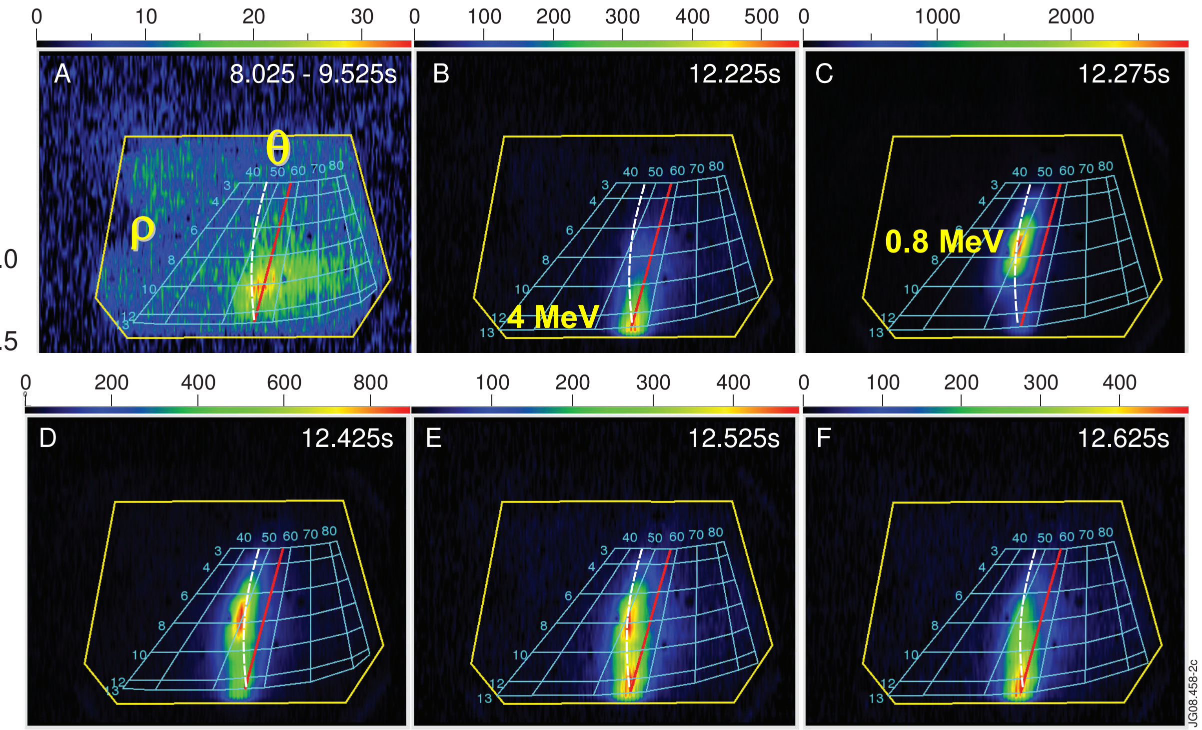

Escaped α-particle diagnostics

5.2. α-particle collectors: Faraday cups in JET

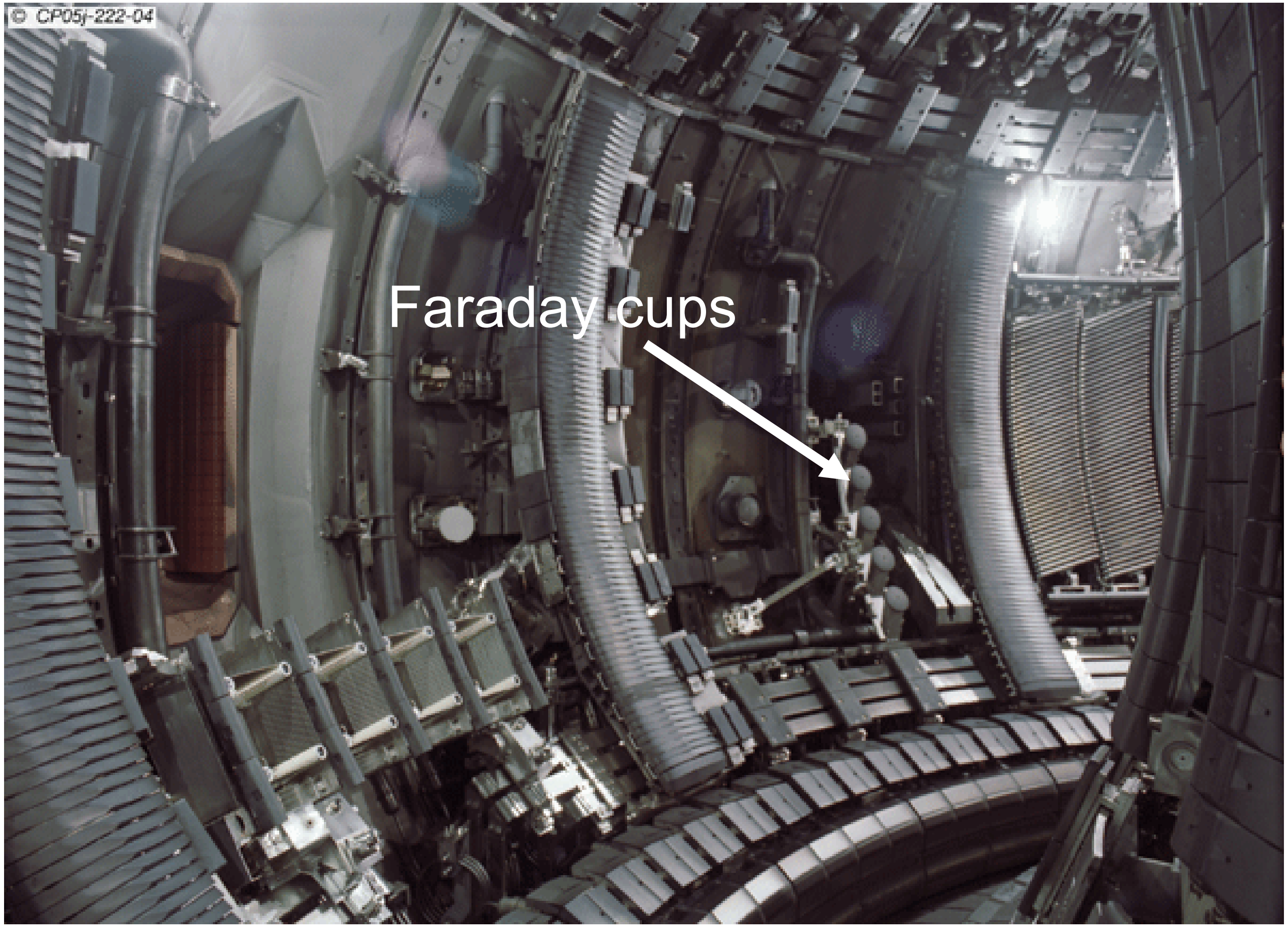

Escaped α-particle diagnostics

5.2. α-particle collectors: Faraday cups position

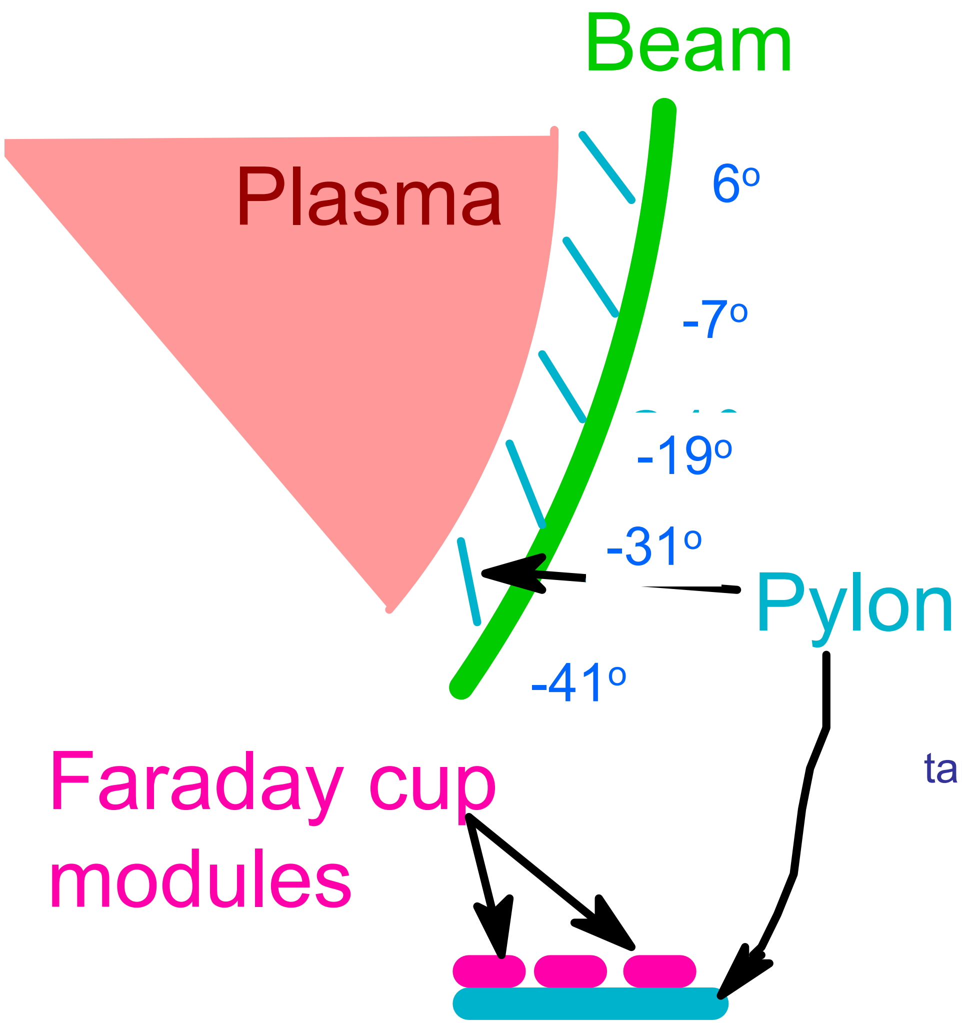

- Curved beam mounted on vessel wall below midplane
- 5 "Pylons" will mount on beam – poloidal resolution
- Each pylon can contain up to 3 Faraday cup modules – radial resolution

$\tan(\theta_{pol})=(Z-Z_0)/(R-R_0)$

$R_0=2.96m,\ Z_0=0$

Escaped α-particle diagnostics

5.2. α-particle collectors: Faraday cup array

Faraday Cups array provides good poloidal and time resolution

- Time resolution: 1 kHz
- Multiple poloidal positions (5)
- Multiple radial locations (max 3)
- Moderate energy resolution (max 8 bins)

- BUT, no pitch angle resolution

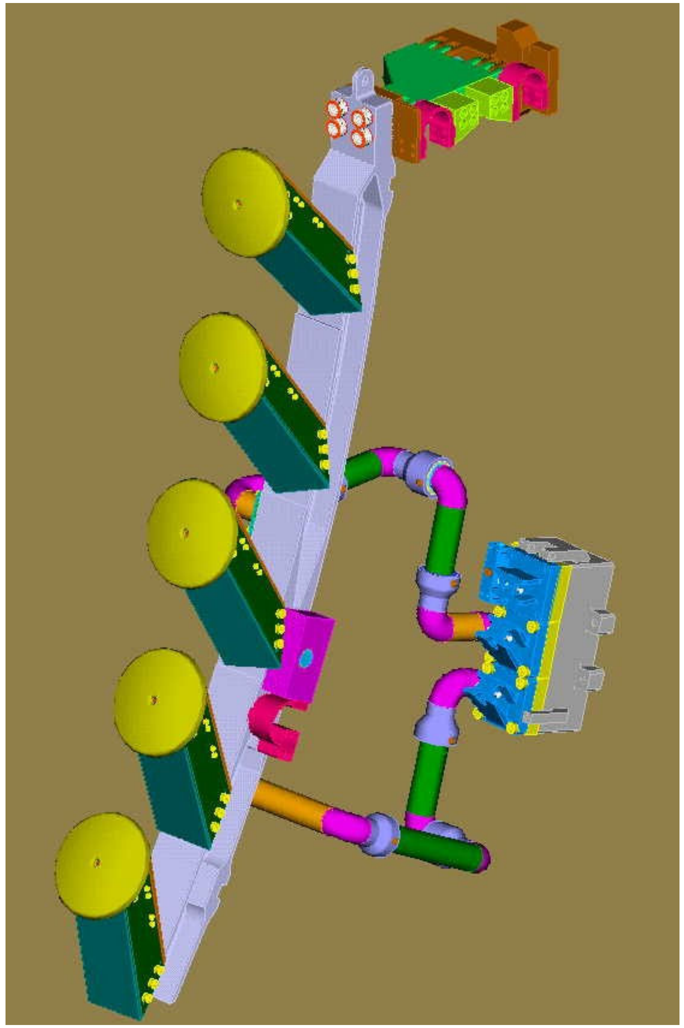

Escaped α-particle diagnostics

5.2. α-particle collectors: Faraday cup assembly

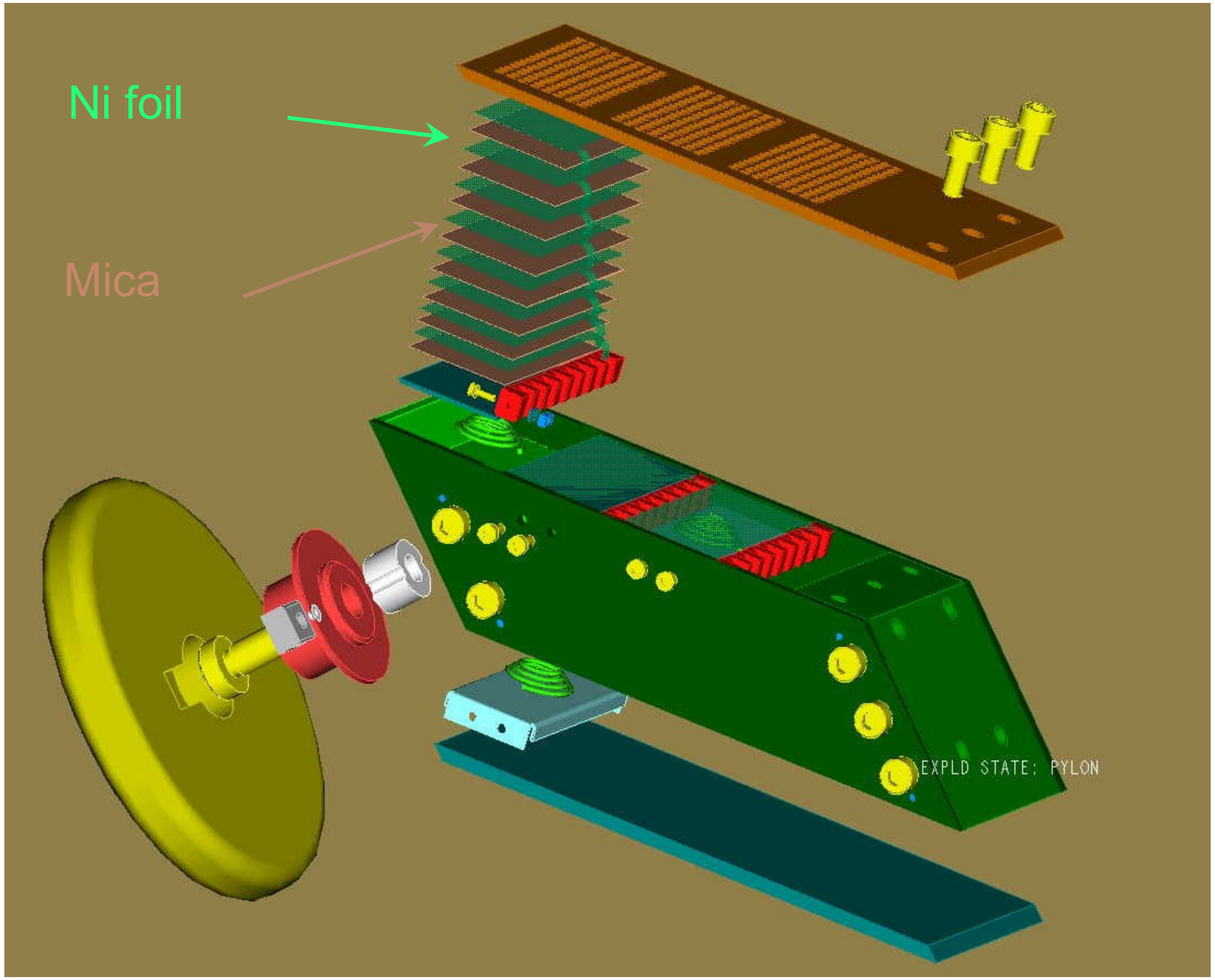

Stack of alternating Ni foils and mica insulating sheets, with terminal block and perforated cover to admit ions.

Escaped α-particle diagnostics

5.2. α-particle collectors: Faraday cup energy resolution

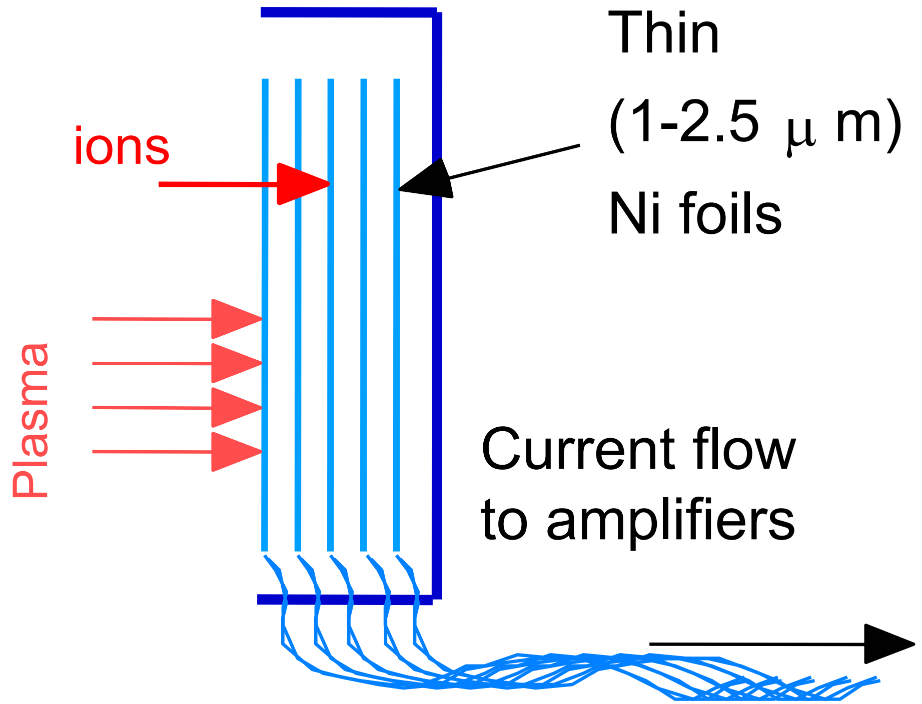

- Detector composed of multiple thin metal foils separated by mica foils
- Ion energy determines deposition depth
- Ion current measured for each foil individually
- Current vs depth gives energy distribution (ΔE~10–50%)

Foils	E_{min}, MeV	E_{max}, MeV
#1	-	1.4
#2	2.0	3.1
#3	3.5	5.0
#4	5.4	6.1

Escaped α-particle diagnostics

5.2. α-particle collectors: Faraday cup results

^{4}He-beam ion acceleration experiment on JET

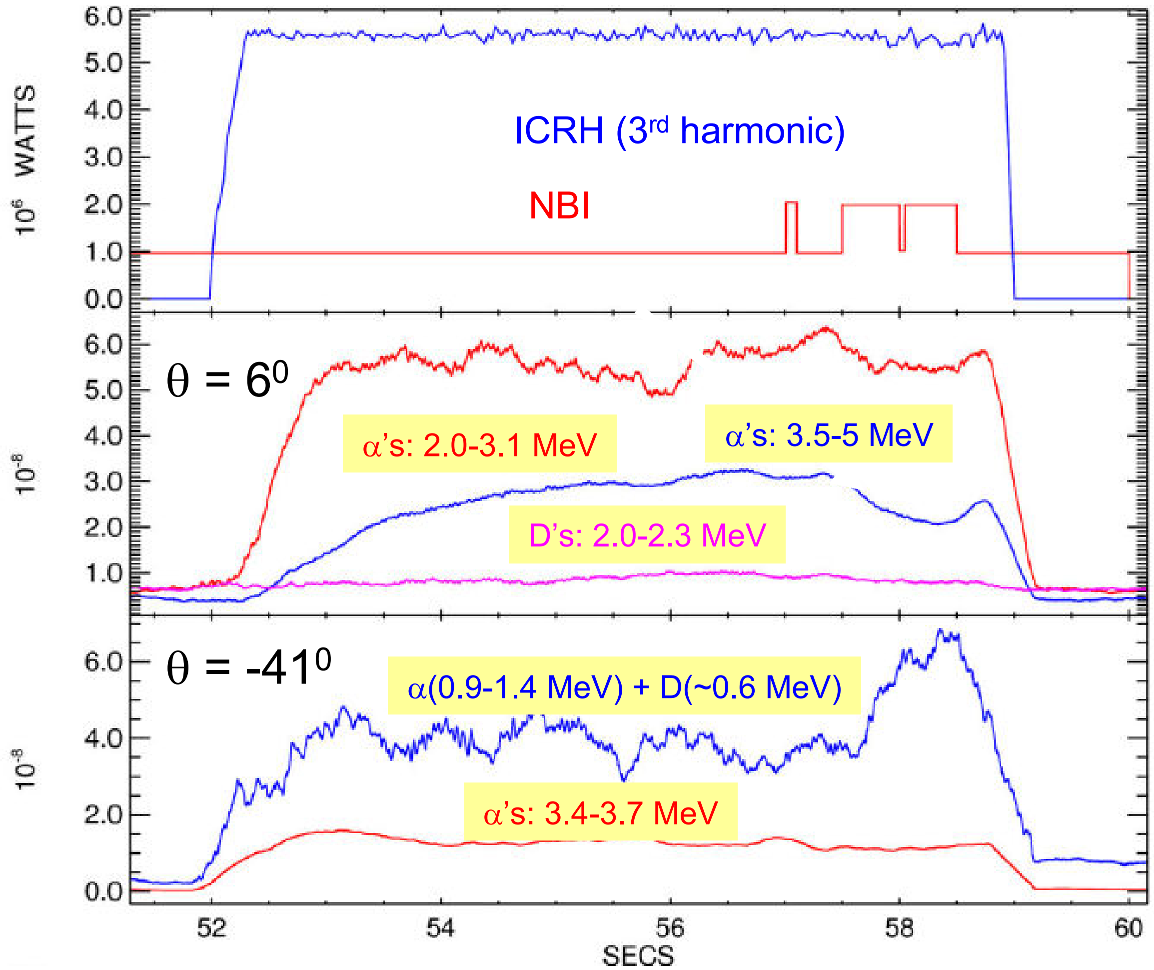

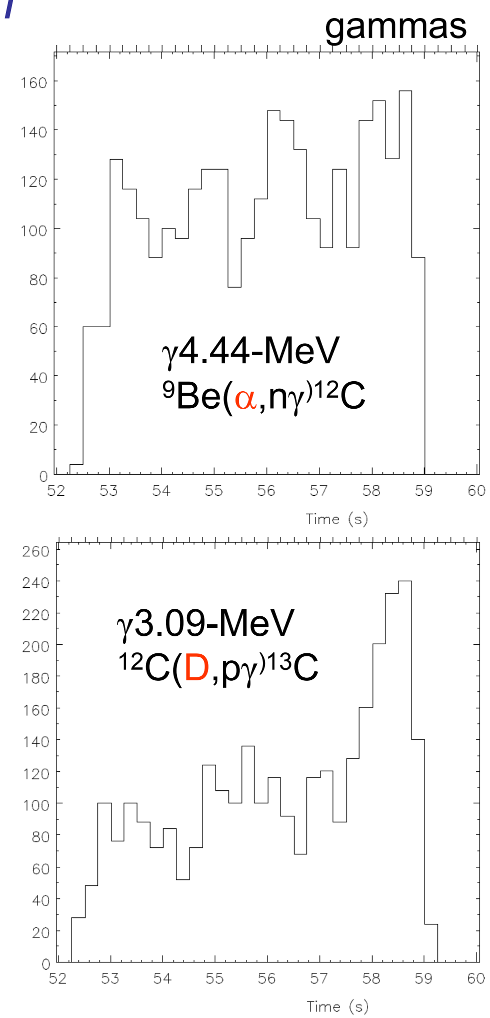

Summary

- Alpha Particle Diagnostics will play important roles in research on self-heating burning plasma physics and in the burn control of the fusion reactors
- An overview of APD based on JET diagnostic set was presented
- Examples of recent JET results were given
- APD play important role for the fast ion physics studies in DD-plasmas and will be crucial for possible next DT-experiments in JET.
- Some of diagnostics from the JET APD set could be used in future DT-experiments in ITER and other burning plasma devices
- Several unique techniques were tested/to be tested at JET in a support of the ITER fast-ion / α-particle diagnostics developments


Thank you very much
for your attention